Published for SISSA by Springer

Received: July 7, 2023
Revised: February 5, 2024
Accepted: February 16, 2024
Published: March 12, 2024

Correlations of C and CP violation in $\eta \to \pi^0\ell^+\ell^-$ and $\eta' \to \eta\ell^+\ell^-$

Hakan Akdag,[a] **Bastian Kubis**[a] **and Andreas Wirzba**[b]

[a] *Helmholtz-Institut für Strahlen- und Kernphysik (Theorie) and Bethe Center for Theoretical Physics, Universität Bonn, 53115 Bonn, Germany*

[b] *Institut für Kernphysik (Theorie), Institute for Advanced Simulation, and Jülich Center for Hadron Physics, Forschungszentrum Jülich, 52425 Jülich, Germany*

E-mail: akdag@hiskp.uni-bonn.de, kubis@hiskp.uni-bonn.de, a.wirzba@fz-juelich.de

Abstract: Based on recent progress in the systematic analysis of C and CP violation in the light-meson sector, we calculate the C-odd transition amplitudes $\eta \to \pi^0\ell^+\ell^-$ and $\eta' \to \eta\ell^+\ell^-$. Focusing on long-distance contributions driven by the lowest-lying hadronic intermediate states, we work out the correlations between these beyond-the-Standard-Model signals and the Dalitz-plot asymmetries in $\eta \to \pi^0\pi^+\pi^-$ and $\eta' \to \eta\pi^+\pi^-$, using dispersion theory.

Keywords: Chiral Lagrangian, Effective Field Theories of QCD, CP Violation, Discrete Symmetries

ArXiv ePrint: 2307.02533

https://doi.org/10.1007/JHEP03(2024)059

JHEP03(2024)059

Contents

1 Introduction

In the recent past new light was shed on analyzing patterns of C- and CP-odd signals in hadronic decays concerning the η-sector. First, ref. [1] provided a new theoretical framework for C violation in $\eta \to \pi^0\pi^+\pi^-$, which was neglected since the 1960s and allows one to decompose the decay amplitude into contributions of different isospin transitions, hence to disentangle the underlying beyond-the-Standard-Model (BSM) operators of isospin $I = 0$ and $I = 2$. This analysis has been improved and extended to $\eta' \to \pi^0\pi^+\pi^-$ as well as $\eta' \to \eta\pi^+\pi^-$ in refs. [2, 3], which relied on the dispersion-theoretical Khuri–Treiman framework. Motivated by these analyses, ref. [4] derived the full set of C- and CP-violating quark-level operators for flavor-conserving, lepton- and baryon-number-preserving transitions in the low-energy effective field theory (LEFT) and matched them onto a T-odd and P-even (ToPe) analog of chiral perturbation theory (ToPeχPT) (cf. also refs. [5, 6]). The latter allows us to access all corresponding C- and CP-odd mesonic interactions.

One may use the formalisms addressed in the previous paragraph to investigate the correlation of T-odd and P-even forces between *different* decays. In this sense we consider C- and CP-violating radiative decays of η and η'. In the following, we denote both mesons

JHEP03(2024)059

branching ratio	SM prediction [17]	experimental limit
$\mathcal{B}(\eta \to \pi^0 e^+ e^-)$	$1.36(15) \times 10^{-9}$	$< 7.5 \times 10^{-6}$ [21]
$\mathcal{B}(\eta \to \pi^0 \mu^+ \mu^-)$	$0.67(7) \times 10^{-9}$	$< 5 \times 10^{-6}$ [19]
$\mathcal{B}(\eta' \to \pi^0 e^+ e^-)$	$3.30(28) \times 10^{-9}$	$< 1.4 \times 10^{-3}$ [20]
$\mathcal{B}(\eta' \to \pi^0 \mu^+ \mu^-)$	$1.81(16) \times 10^{-9}$	$< 6 \times 10^{-5}$ [19]
$\mathcal{B}(\eta' \to \eta e^+ e^-)$	$0.50(4) \times 10^{-9}$	$< 2.4 \times 10^{-3}$ [20]
$\mathcal{B}(\eta' \to \eta \mu^+ \mu^-)$	$0.240(21) \times 10^{-9}$	$< 1.5 \times 10^{-5}$ [19]

Table 1. Standard-Model predictions for dilepton branching ratios based on the C-even two-photon mechanism [17], as well as corresponding experimental upper limits. Note that below only the cases $\eta \to \pi^0 \ell^+ \ell^-$ and $\eta' \to \eta \ell^+ \ell^-$ will be considered further.

with $\eta^{(\prime)}$. Given that $\eta^{(\prime)}$ as well as π^0 have the eigenvalue $C = +1$ but photons have $C = -1$, C is violated in general if $\eta^{(\prime)}$ decays into an arbitrary number of uncharged pions and an *odd* number of photons. This consideration also holds for radiative decays of the η' into an η. In the following we will focus on the radiative C-odd decays $\eta \to \pi^0 \gamma^{(*)}$ and $\eta' \to \eta \gamma^{(*)}$. To shorten the notation we will refer to both processes collectively by $X \to Y \gamma^{(*)}$. Angular momentum conservation demands the final state to be in a relative P-wave. Consequently, parity is conserved and the decays at hand additionally violate CP, thus offering an opportunity to investigate ToPe forces. The decay into a real, transverse photon violates both gauge invariance and the conservation of angular momentum [7, 8]. Therefore, the focus shall be laid on $X \to Y \gamma^* \to Y \ell^+ \ell^-$, where the off-shell photon decays subsequently into a pair of charged leptons. At the theoretical front, the investigation of this BSM one-photon exchange urgently requires an update [9, 10] in comparison to analyses of the SM contribution, cf. refs. [11–17], as well as studies of other BSM effects in these decays [8, 18]. From an experimental point of view, bounds on all the leptonic channels have already been set [19–21] and may become more stringent in future measurements [22–28].

We summarize the currently most stringent experimental upper bounds on the $X \to Y \ell^+ \ell^-$ branching ratios in table 1, and contrast them with the corresponding SM predictions based on the C-conserving two-photon mechanism [17]. We observe that those predictions are below the current limits by large factors, between 5×10^3 (for $\eta \to \pi^0 e^+ e^-$) and 5×10^6 (for $\eta' \to \eta e^+ e^-$). We will therefore perform the analysis in the following in the spirit that we assume the SM contribution to be small, and any observable or observed signal to be a sign of a C-odd single-photon mechanism.[1] Note furthermore that C-even and C-odd amplitudes cannot interfere on the level of the branching ratio; such interference effects could only induce Dalitz-plot asymmetries (cf. refs. [1–3]), which would only be sizable if both amplitudes are of comparable magnitude. We therefore refrain from discussing such interference effects in any detail.

[1] Similarly, we disregard other potential BSM effects, such as of CP-even weakly coupled scalars; see, e.g., ref. [8] and references therein.

JHEP03(2024)059

We emphasize the special role of CP violation in flavor-*conserving* transitions such as all η and η' decays discussed here. In contrast to similar kaon decays $K \to \pi\ell^+\ell^-$ [29, 30], SM CP-odd contributions induced by the weak interactions are very strongly suppressed, as any weak phase cancels at one loop, and any such contribution only depends on the squared moduli of the Cabibbo–Kobayashi–Maskawa (CKM) matrix elements. This is not unlike the situation for electric dipole moments of nucleons, which are considered quasi-free of any CKM-matrix-induced SM background [31–34].

Assuming that the underlying new physics generating the C- and CP-odd decays $X \to Y\ell^+\ell^-$ originates from sources at some high-energy scale Λ, there are in principle three dominant mechanisms to consider:

1. short-distance contributions to the dilepton final state,
2. long-distance contributions caused by C- and CP-odd photon–hadron couplings,
3. long-distance contributions induced by hadronic intermediate states.

For the first two classes we rely on ToPeχPT as proposed in ref. [4]. One intricacy of the contribution by hadronic intermediate states is that the subsequent photon is allowed to have both isoscalar and isovector components. To predict the involved isovector transitions in a model-independent way, one can utilize the $X \to Y\pi^+\pi^-$ amplitudes derived non-perturbatively in the Khuri–Treiman framework [2, 3] and establish dispersion relations for the respective transition form factors.[2] Analogous relations have previously been derived for the decays ω, ϕ, $J/\psi \to \pi^0\gamma^*$ [36–40], which are compatible with conservation of all discrete symmetries. In addition, we sketch an idea of how to evaluate the isoscalar contribution of the photon, employing a less sophisticated, but still symmetry-driven, vector-meson-dominance (VMD) model for the decay $X \to Y\gamma^*$. By an analytic continuation of the three-body amplitudes $X \to Y\pi^+\pi^-$ to the second Riemann sheet we can extract ρYX couplings, which can be related to the relevant ones with the same total isospin in the VMD model using $SU(3)$ symmetry and naive dimensional analysis (NDA).

To extract observables of the C- and CP-violating contribution in $X \to Y\ell^+\ell^-$ driven by a one-photon exchange we pursue the following strategy. First, we consider the phenomenology behind the three mechanisms mentioned above in section 2. For this purpose we lay out the basic definitions of kinematics and relate the amplitude to the (differential) decay widths in section 2.1. We discuss the short-range semi-leptonic operators, the long-range direct photon–hadron couplings, and the long-range hadronic contributions on a general level in sections 2.2–2.4, respectively. Subsequently, section 2.5 includes a discussion of the feasibility of these contributions. The remainder of the article solely focuses on long-distance contributions with hadronic intermediate states. In section 3 we investigate the isovector contributions to these hadronic long-range effects. For this purpose, we first sketch the C- and CP-odd contributions to the decays $X \to Y\pi^+\pi^-$ in section 3.1, which serve as input to the respective transition form factors. The computation of the latter is discussed

[2]This relation is the reason why we largely ignore $\eta' \to \pi^0\ell^+\ell^-$ in this article: the corresponding hadronic decay $\eta' \to \pi^0\pi^+\pi^-$ is comparatively rare, such that no useful limits on C violation therein can be derived so far [2, 3, 35].

JHEP03(2024)059

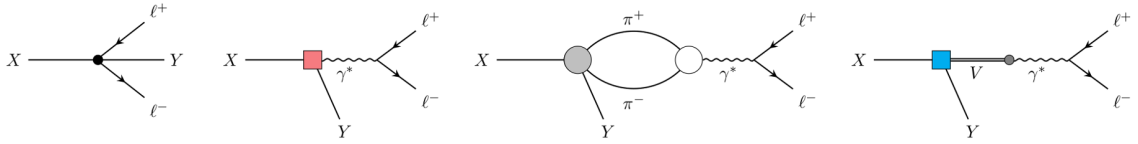

Figure 1. Contributions to the C- and CP-odd decay $X \to Y\ell^+\ell^-$. The first diagram describes a short-range semi-leptonic four-point vertex, the second one includes a long-range hadron–photon coupling, while the last two diagrams account for possible hadronic intermediate states. Among the latter, the pion loop corresponds to an isovector transition while the vector-meson conversion respects the isoscalar part of the virtual photon. The black dot, the red box, the gray circle, and the blue box refer to different C- and CP-violating vertices, while the white circle is C- and CP-conserving.

in section 3.2. In section 3.3, we extract the corresponding C-odd couplings of the $\rho(770)$ resonance to $\eta\pi^0$ and $\eta'\eta$ by analytic continuation in the complex-energy plane. Subsequently, we estimate the size of the hadronic long-range effects in the isoscalar parts in section 4. Finally, we present the predicted upper limits on the branching ratios in section 5 and close with a short summary and outlook in section 6.

2 Phenomenology

In this section we discuss the phenomenological importance of the three mechanisms driving $X \to Y\ell^+\ell^-$ and provide the model-independent expressions for them. As an illustration we depict the different contributions in figure 1. For simplicity we adapt the notation and conventions introduced for the construction of operators in ToPeχPT in ref. [4] without further details.

2.1 Kinematics

Consider the transition amplitude $X(P) \to Y(p)\ell^+(p_{\ell^+})\ell^-(p_{\ell^-})$, with two pseudoscalars X and Y of masses $M_X > M_Y$. Conventionally, we describe the three-body decay in terms of the Lorentz invariants

$$s = (P-p)^2, \qquad t_\ell = (P-p_{\ell^+})^2, \qquad u_\ell = (P-p_{\ell^-})^2. \tag{2.1}$$

With the electromagnetic quark current

$$J_\mu = \sum_f Q_f \bar{q}_f \gamma_\mu q_f \,, \tag{2.2}$$

where Q_f indicates the electric charge of the respective quarks with flavor f and is conventionally used in units of the proton charge e, the singularity-free electromagnetic transition form factor $F_{XY}(s)$ in $X \to Y\gamma^*$ can be decomposed by Poincaré invariance and current conservation as [9, 30]

$$\langle Y(p)|J_\mu(0)|X(P)\rangle = -i\left[s(P+p)_\mu - (P^2-p^2)q_\mu\right] F_{XY}(s) \equiv -iQ_\mu F_{XY}(s)\,. \tag{2.3}$$

Here we introduced the photon's momentum $q_\mu = (P-p)_\mu$. Note that $F_{XY}(s)$ thus defined is real at leading order in ToPeχPT.[3] Upon contraction with the lepton current the full

[3]Put differently, $F_{XY}(s)$ is real below the onset of cuts or imaginary parts due to hadronic intermediate states, i.e., for $s \leq 4M_\pi^2$.

JHEP03(2024)059

decay amplitude becomes

$$i\mathcal{M}(X \to Y\ell^+\ell^-) = e^2\,(P+p)_\mu F_{XY}(s)\,\bar{u}_r(p_{\ell^-})\gamma^\mu v_{r'}(p_{\ell^+}), \tag{2.4}$$

where the term proportional to q_μ drops out due to current conservation [9]. In the course of this work, we will see explicitly that the amplitude of each mechanism restores this functional form. Taking the squared absolute value and summing over the lepton spins, one may obtain the doubly differential decay width [41]

$$\frac{\mathrm{d}\Gamma(X \to Y\ell^+\ell^-)}{\mathrm{d}s\,\mathrm{d}\tau} = \frac{\alpha^2}{16\pi M_X^3}\left(\lambda(s, M_X^2, M_Y^2) - \tau^2\right)|F_{XY}(s)|^2, \tag{2.5}$$

in terms of the electromagnetic fine-structure constant $\alpha = e^2/4\pi$, the Källén function $\lambda(x,y,z) = x^2+y^2+z^2-2(xy+xz+yz)$, and the Lorentz invariant $\tau = t_\ell - u_\ell$. The τ-integration can be carried out analytically, giving

$$\frac{\mathrm{d}\Gamma(X \to Y\ell^+\ell^-)}{\mathrm{d}s} = \frac{\alpha^2}{8\pi M_X^3}\,\lambda^{3/2}(s, M_X^2, M_Y^2)\,\sigma_\ell(s)\left(1 - \frac{\sigma_\ell^2(s)}{3}\right)|F_{XY}(s)|^2, \tag{2.6}$$

where $\sigma_\ell(s) = \sqrt{1-4m_\ell^2/s}$ and the physical range is restricted to $s \in (4m_\ell^2, (M_X - M_Y)^2)$. Throughout, we use the masses $m_e = 0.51\,\mathrm{MeV}$, $m_\mu = 105.66\,\mathrm{MeV}$, $M_\eta = 547.86\,\mathrm{MeV}$, $M_{\eta'} = 957.78\,\mathrm{MeV}$, $M_{\pi^\pm} = 139.57\,\mathrm{MeV}$, and $M_{\pi^0} = 134.98\,\mathrm{MeV}$ [42]. For later use, we also quote the vector-meson masses $M_\omega = 782.66\,\mathrm{MeV}$ [42] and $M_\rho = 763.7\,\mathrm{MeV}$, where the latter is the real value of the $\rho(770)$-meson pole as determined in ref. [43]. The errors and additional decimal digits on all of these masses are negligible in our analysis.

2.2 Direct semi-leptonic contributions to $X \to Y\ell^+\ell^-$

In ref. [4] it was shown that the only C-odd, P-even semi-leptonic four-point vertex to $\eta \to \pi^0\ell^+\ell^-$ at lowest order in the QED fine-structure constant and soft momenta originates from the dimension-8 LEFT operator

$$\mathcal{O}_{\ell\psi}^{(u)} \equiv \frac{c_{\ell\psi}^{(u)}}{\Lambda^4}\,\bar{\ell}\gamma^\mu\ell\bar{\psi}\gamma^\nu T^a\psi G_{\mu\nu}^a\,, \tag{2.7}$$

where $c_{\ell\psi}^{(u)}$ denotes flavor-dependent Wilson coefficients.[4] The choice of the high-energy scale Λ depends on the interpretation of the ToPe operators: in the picture of LEFT, Λ can be in the order of the electroweak scale, while in the spirit of the Standard Model effective field theory Λ is a typical BSM scale. The respective leading ToPeχPT operators in the large-N_c limit read [4]

$$\bar{X}_{\ell\psi}^{(u)} \supset \frac{c_{\ell\psi}^{(u)}}{\Lambda^4}\,\bar{g}_1^{(u)}\,i\varphi\langle\lambda_L\partial_\mu\bar{U}^\dagger\bar{U} - \lambda_R\partial_\mu\bar{U}\bar{U}^\dagger\rangle\bar{\ell}\gamma^\mu\ell\,, \tag{2.8}$$

[4] In contrast, CP-violating quark–lepton operators that contribute to these decays but are C-even and P-odd already appear at dimension 6 [18, 44]. Note furthermore that this suppression is specific for flavor-diagonal transitions: flavor-changing processes of C- and CP-odd nature are similarly already generated at dimension 6 [5, 29].

JHEP03(2024)059

where we employ the simple single-angle η-η' mixing scheme [45], for which the singlet component corresponds to

$$\varphi = \frac{\sqrt{2}}{3\sqrt{3}F_0}\,\eta + \frac{4}{3\sqrt{3}F_0}\,\eta'\,. \tag{2.9}$$

The meson matrix in the large-N_c limit is then given by

$$\bar{U} = \exp\left(\frac{i\bar{\Phi}}{F_0}\right), \quad \text{where} \quad \bar{\Phi} = \begin{pmatrix} \frac{1}{\sqrt{3}}\eta' + \sqrt{\frac{2}{3}}\eta + \pi^0 & \sqrt{2}\pi^+ & \sqrt{2}K^+ \\ \sqrt{2}\pi^- & \frac{1}{\sqrt{3}}\eta' + \sqrt{\frac{2}{3}}\eta - \pi^0 & \sqrt{2}K^0 \\ \sqrt{2}K^- & \sqrt{2}\bar{K}^0 & \frac{2}{\sqrt{3}}\eta' - \sqrt{\frac{2}{3}}\eta \end{pmatrix}. \tag{2.10}$$

In both eqs. (2.9) and (2.10), η and η' refer to the physical fields; see, e.g., refs. [45–47] for detailed discussions on more elaborate mixing schemes. Furthermore, in relation (2.8) we have introduced the spurion matrices $\lambda_{L,R}$ in flavor space, which were defined in ref. [4] and acquire the same physical values, namely $\lambda_{L,R} \in \{\mathrm{diag}(1,0,0), \mathrm{diag}(0,1,0), \mathrm{diag}(0,0,1)\}$ for the quark flavor $\psi = u, d, s$, respectively. Besides, F_0 denotes the common meson decay constant in the combined chiral and large-N_c limit, $F_0 \lesssim F_\pi \approx 92.3\,\mathrm{MeV}$. Summing over ψ and only picking the interactions relevant for our interests, the operator $\bar{X}^{(u)}_{\ell\psi}$ gives rise to the leading-order Lagrangians

$$\mathcal{L}_{XY\ell^+\ell^-} = \frac{1}{\Lambda^4 F_0^2}\,\mathcal{N}_{X\to Y\ell^+\ell^-}\,\bar{\ell}\gamma^\mu \ell X \partial_\mu Y \tag{2.11}$$

with the normalizations

$$\mathcal{N}_{\eta\to\pi^0\ell^+\ell^-} \equiv \frac{2\sqrt{2}}{3\sqrt{3}}\,\bar{g}_1^{(u)}\,(c_{\ell u}^{(u)} - c_{\ell d}^{(u)})\,, \qquad \mathcal{N}_{\eta'\to\eta\ell^+\ell^-} \equiv \frac{2\sqrt{2}}{3}\,\bar{g}_1^{(u)}\,(c_{\ell u}^{(u)} + c_{\ell d}^{(u)} - 2c_{\ell s}^{(u)})\,. \tag{2.12}$$

Both processes are uncorrelated as their normalizations are linearly independent; the flavor combinations reflect the isospin and $SU(3)$ structure of the transitions. Making use of the Dirac equation for the leptons, the corresponding matrix element yields

$$i\mathcal{M} = e^2 (P+p)_\mu F_1(s)\,\bar{u}_r(p_{\ell^-})\gamma^\mu v_{r'}(p_{\ell^+})\,, \tag{2.13}$$

with

$$F_1(s) \equiv -\frac{1}{2e^2\Lambda^4 F_0^2}\,\mathcal{N}_{X\to Y\ell^+\ell^-} \sim -\frac{1}{\Lambda^4}\frac{2\pi F_0^2}{e^2} = -\frac{F_0^2}{2\alpha\Lambda^4}\,. \tag{2.14}$$

In the last step we applied the NDA assumption $\mathcal{N}_{X\to Y\ell^+\ell^-} \sim 4\pi F_0^4$. Note, however, that the sign of the normalization is not fixed by NDA.

2.3 Direct photonic contributions to $X \to Y\gamma^*$

The leading-order contribution to the effective Lagrangian of $X \to Y\gamma^*$ reads [4]

$$\mathcal{L}_{X\to Y\gamma^*} = \frac{1}{\Lambda^4 F_0^2}\mathcal{N}_{X\to Y\gamma^*}\partial_\mu X \partial_\nu Y F^{\mu\nu} + \mathcal{O}(p^6). \tag{2.15}$$

We may access the normalization $\mathcal{N}_{X\to Y\gamma^*}$ using NDA, by regarding the possible sources on the level of LEFT, cf. ref. [4]. In this discussion we can directly ignore LEFT sources whose

JHEP03(2024)059

leading-order contributions in ToPeχPT are proportional to the ϵ-tensor and can thus not generate an even number of pseudoscalars and at the same time preserve parity. The NDA estimate of $\mathcal{N}_{X\to Y\gamma^*}$ for the chirality-breaking dimension-7 LEFT quark-quadrilinear [48–52]

$$\mathcal{O}^{(a)}_{\psi\chi} = \frac{v}{\Lambda^4} c^{(a)}_{\psi\chi}\, \bar{\psi}\overleftrightarrow{D}_\mu \gamma_5 \psi \bar{\chi}\gamma^\mu\gamma_5\chi\,, \tag{2.16}$$

which is in the focus of ref. [4], yields $evF_0^3/4\pi$, with Higgs vev v. For the C- and CP-odd dimension-8 operators listed in this reference with two quarks and two gluon field strengths, four quarks and one gluon field strength, four quarks and one photon field strength, we have $\mathcal{N}_{X\to Y\gamma^*} \sim eF_0^4$, $eF_0^4/(4\pi)$, F_0^4, respectively. It has to be underlined that *each* of these estimates may differ by one order of magnitude, possibly rendering all of these operators to the same numerical size. However, in the scope of these NDA estimations, we assume the normalization of the dimension-7 LEFT operator to dominate the remaining ones.

Using $\mathcal{L}_{X\to Y\gamma^*}$ to evaluate the C-odd vertex in the second diagram of figure 1, we obtain the matrix element [4]

$$i\mathcal{M} = e^2(P+p)_\nu F_2(s)\, \bar{u}_r(p_{\ell^-})\gamma^\nu v_{r'}(p_{\ell^+})\,, \tag{2.17}$$

with

$$F_2(s) \equiv \frac{1}{2e\Lambda^4 F_0^2}\mathcal{N}_{X\to Y\gamma^*} \sim \frac{vF_0}{8\pi\Lambda^4}\,. \tag{2.18}$$

Again, NDA does not provide any information on the sign of the amplitude. Comparing eqs. (2.14) and (2.18), we note $F_2(s)/F_1(s) \sim \alpha v/(4\pi F_0) \approx 1.5$, hence both contributions are really expected to be of comparable size.

2.4 Hadronic long-range effects

The hadronic long-range contributions to the transition form factor can be constructed with knowledge about ToPe forces in $X \to Y\pi^+\pi^-$ [2, 3]. We consider in the following sections both the isovector and isoscalar part of the photon.

2.4.1 The isovector contribution

In this section we establish dispersion relations for hadronic contributions of the C- and CP-odd transition form factor F_{XY} and restrict the calculation to the isovector part of the photon. The discontinuity of $X \to Y\gamma^*$, as depicted in figure 2, can be calculated by applying a unitarity cut on the dominant intermediate state, i.e., two charged pions, allowing us to access the transition form factor in a non-perturbative fashion. The first ingredient to the discontinuity in figure 2 is indicated by the gray blob and describes the C- and CP-odd contributions to the hadronic $X \to Y\pi^+\pi^-$ decay amplitude defined by

$$\langle Y(p)\,\pi^+(p_+)\,\pi^-(p_-)|iT|X(P)\rangle = (2\pi)^4\,\delta^{(4)}(P-p-p_+-p_-)\,i\mathcal{M}^{XY}(s,t,u)\,. \tag{2.19}$$

These amplitudes will be discussed in detail for the different cases in section 3. The remaining contribution is the pion vector form factor defined via the current[5]

$$\langle\pi^+(p_+)\pi^-(p_-)|J_\mu(0)|0\rangle = (p_+-p_-)_\mu F_\pi^V(s)\,. \tag{2.20}$$

[5]In the isospin limit, which we will employ for the pion form factor in the following, only the isovector contribution of the current contributes, i.e., $J^{(1)}_\mu = \frac{1}{2}\big(\bar{u}\gamma_\mu u - \bar{d}\gamma_\mu d\big)$.

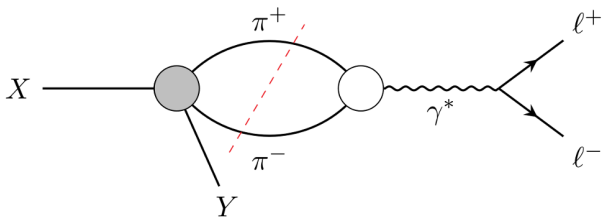

Figure 2. Discontinuity of the $X \to Y\gamma^*$ transition form factors, representative for the decays $\eta \to \pi^0\gamma^*$ and $\eta' \to \eta\gamma^*$. The white blob denotes the pion vector form factor and the gray one the C-violating contributions to the $\eta \to \pi^0\pi^+\pi^-$ and $\eta' \to \eta\pi^+\pi^-$ amplitudes, respectively. The dashed line illustrates the unitarity cut.

Note that this equation and eq. (2.3) differ, beside the respective momentum configuration, by an explicit imaginary unit as demanded by their different behavior under time reversal. With only elastic rescattering taken into account, the pion vector form factor obeys the discontinuity relation

$$\text{disc}\, F_\pi^V(s) = 2i\, F_\pi^V(s) \sin\delta_1(s) e^{-i\delta_1(s)} \theta(s - 4M_\pi^2)\,, \tag{2.21}$$

where $\delta_1(s)$ denotes the P-wave $\pi\pi$ phase shift with two-body isospin $I_{\pi\pi} = 1$. The most general solution to this equation is given in terms of the Omnès function [53]

$$F_\pi^V(s) = P_n(s)\,\Omega_1(s) = P_n(s) \exp\left(\frac{s}{\pi} \int_{4M_\pi^2}^{\infty} \frac{\delta_1(x)}{x(x-s)}\, \mathrm{d}x\right), \tag{2.22}$$

with a real-valued subtraction polynomial P_n of order n. The index of the Omnès function indicates the isospin $I_{\pi\pi}$ of the dipion state. The pion vector form factor is expected to behave as $F_\pi^V(s) \asymp 1/s$ for large energies [54–61] (up to logarithmic corrections), and to be free of zeros [61, 62]. Thus, P_n is a constant and can be set to 1 due to gauge invariance, such that $F_\pi^V(s) = \Omega_1(s)$. For consistency we waive the incorporation of inelastic effects, which we do not consider in $X \to Y\pi^+\pi^-$ either. In the region of the $\rho(770)$ resonance dominating $F_\pi^V(s)$, these are known to affect the form factor by no more than 6%, depending on the phase shift used as input [63]. Given other sources of uncertainty in the present study, we consider this error negligible.

When we cut the dipion intermediate state in figure 2, the discontinuity of the isovector contribution $F_{XY}^{(1)}$ to the transition form factor F_{XY} becomes

$$Q_\mu \text{disc} F_{XY}^{(1)}(s) = \int \frac{\mathrm{d}^4k}{(2\pi)^2}\, \delta(k^2 - M_\pi^2)\, \delta\left((q-k^2) - M_\pi^2\right)\, \mathcal{M}^{XY}(s,t,u)\, (q-2k)_\mu F_\pi^{V*}(s)\,, \tag{2.23}$$

where $t = (P - p_+)^2$ and $u = (P - p_-)^2$. We find

$$\text{disc} F_{XY}^{(1)}(s) = -\frac{1}{24\pi} \sigma_\pi^3(s) F_\pi^{V*}(s)\, f_{XY}(s)\, \theta(s - 4M_\pi^2)\,, \tag{2.24}$$

where $\sigma_\pi(s) = \sqrt{1 - 4M_\pi^2/s}$. In this discontinuity relation the quantity f_{XY} denotes the P-wave projection of the hadronic decay amplitude given by

$$f_{XY}(s) \equiv \frac{3}{2\kappa(s)} \int_{-1}^{1} \mathrm{d}z\, z\, \mathcal{M}^{XY}(s,t,u), \tag{2.25}$$

JHEP03(2024)059

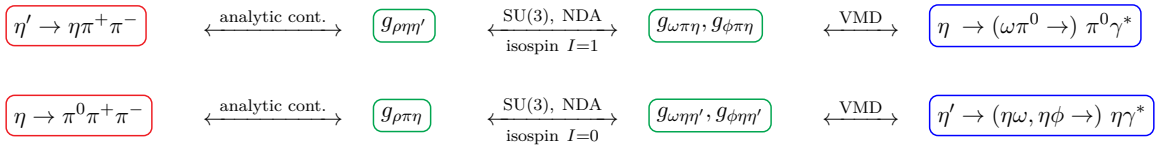

Figure 3. Schematic sketch of the strategy to extract the isoscalar contribution of the $\eta \to \pi^0\gamma^*$ ($\eta' \to \eta\gamma^*$) transition form factor (blue) from the C- and CP-odd $\eta' \to \eta\pi^+\pi^-$ ($\eta \to \pi^0\pi^+\pi^-$) amplitude (red) using vector-meson couplings (green).

with

$$z = \frac{t-u}{\kappa(s)} \quad \text{and} \quad \kappa(s) = \sigma_\pi(s)\lambda^{1/2}(s, M_X^2, M_Y^2)\,. \tag{2.26}$$

Adapting the high-energy behavior of f_{XY} and δ_1 from refs. [2, 3], an unsubtracted dispersion relation is sufficient to ensure convergence of the remaining integral over the discontinuity, such that the form factor can be evaluated with

$$F_{XY}^{(1)}(s) = \frac{i}{48\pi^2}\int_{4M_\pi^2}^{\infty} \mathrm{d}x\, \sigma_\pi^3(x) F_\pi^{V*}(x)\, \frac{f_{XY}(x)}{x-s}. \tag{2.27}$$

2.4.2 The isoscalar contribution

In order to estimate the isoscalar contribution, we apply a VMD pole approximation and consider a vector-meson conversion of γ^* to v_μ, with $v \in \{\omega, \phi\}$, cf. the very right diagram in figure 1. While this strategy is not as model-independent and sophisticated as the dispersive analysis of the isovector part of γ^*, it serves as a good approximation to at least estimate the relative size of this contribution, not least due to the narrowness of the ω and ϕ resonances dominating isoscalar vector spectral functions at low energies. Furthermore, this ansatz even correlates the decay $\eta \to \pi^0\gamma^*$ to $\eta' \to \eta\pi^+\pi^-$ and $\eta' \to \eta\gamma^*$ to $\eta \to \pi^0\pi^+\pi^-$ by following the strategy sketched in figure 3 to relate the decays of same total isospin.

The combination of vector mesons with χPT was extensively worked out for instance in refs. [64–69] and references therein. The number of free parameters can be reduced most efficiently, cf. ref. [66], by coupling uncharged vector mesons to uncharged pseudoscalars via the field-strength tensor $V_{L,R}^{\mu\nu}$. The latter is the analog to the photonic one with the same discrete symmetries and transformations under $SU(3)_L \times SU(3)_R$. If we only consider the relevant degrees of freedom, i.e., treating $\bar{U}$ and $V_{L,R}^\mu$ as diagonal matrices, we can effectively write

$$V_{L,R}^{\mu\nu} = \partial^\mu V_{L,R}^\nu - \partial^\nu V_{L,R}^\mu\,. \tag{2.28}$$

The physical value of this chiral building block can be evaluated with $V_L^\mu = V_R^\mu = \mathrm{diag}(\rho + \omega, -\rho + \omega, \sqrt{2}\phi)^\mu + \ldots$, where the ellipsis indicates terms without vector mesons. At the mesonic level, we can deduce the desired interaction from the leading-order $XY\gamma^*$ operator, cf. ref. [10], and hence write

$$\mathcal{L}_{vYX} = g_{vYX}\partial_\mu X \partial_\nu Y v^{\mu\nu}\,, \tag{2.29}$$

JHEP03(2024)059

with $v_{\mu\nu} \equiv \partial_\mu v_\nu - \partial_\nu v_\mu$. The ToPe$\chi$PT operators that can generate this mesonic interaction at leading order in the large-N_c power counting, i.e., $\mathcal{O}(p^4, \delta^2)$ (see ref. [4] for further details), and originate from the LEFT operator in eq. (2.16) are

$$\begin{aligned}\bar{X}^{(a)}_{\psi\chi} \supset \frac{v}{\Lambda^4} c^{(a)}_{\psi\chi} \Big(& \bar{g}^{(a)}_{V_1} \langle \lambda_L \partial_\nu \bar{U}^\dagger \bar{U} - \lambda_R \partial_\nu \bar{U} \bar{U}^\dagger \rangle \langle (\lambda V_L^{\mu\nu} \partial_\mu \bar{U}^\dagger - \lambda^\dagger V_R^{\mu\nu} \partial_\mu \bar{U}) - \text{h.c.} \rangle \\ & + \bar{g}^{(a)}_{V_2} \langle \lambda \partial_\mu \bar{U}^\dagger - \lambda^\dagger \partial_\mu \bar{U} \rangle \langle (\lambda_L V_L^{\mu\nu} \partial_\nu \bar{U}^\dagger \bar{U} - \lambda_R V_R^{\mu\nu} \partial_\nu \bar{U} \bar{U}^\dagger) - \text{h.c.} \rangle \\ & + \bar{g}^{(a)}_{V_3} \partial_\nu \varphi \langle (\lambda \lambda_L V_L^{\mu\nu} \partial_\mu \bar{U}^\dagger - \lambda^\dagger \lambda_R V_R^{\mu\nu} \partial_\mu \bar{U}) - \text{h.c.} \rangle \Big) \,. \end{aligned} \tag{2.30}$$

Here, we only list the operators leading to distinct, non-vanishing, expressions after we set $\lambda^{(\dagger)}$, $\lambda_{L,R}$, and $V^{\mu\nu}_{L,R}$ to their physical values and use the fact that in our application all appearing matrices are diagonal and therefore commute. Evaluating the flavor traces of the operator in the first line and labeling the vector-meson couplings with a corresponding superscript (V_1), we end up with

$$\begin{aligned} g^{(V_1)}_{\rho\pi\eta} &= \frac{16v}{\Lambda^4 F_0^2} \sqrt{\frac{2}{3}} (c^{(a)}_{ud} + c^{(a)}_{du}) \bar{g}^{(a)}_{V_1} - \frac{1}{\sqrt{3}} g^{(V_1)}_{\omega\eta\eta'} \,, & g^{(V_1)}_{\rho\eta\eta'} &= \frac{8\sqrt{2}v}{\Lambda^4 F_0^2} (c^{(a)}_{us} - c^{(a)}_{ds}) \bar{g}^{(a)}_{V_1} \,, \\ g^{(V_1)}_{\omega\pi\eta} &= \frac{16v}{\Lambda^4 F_0^2} \sqrt{\frac{2}{3}} (c^{(a)}_{ud} - c^{(a)}_{du}) \bar{g}^{(a)}_{V_1} - \frac{1}{\sqrt{3}} g^{(V_1)}_{\rho\eta\eta'} \,, & g^{(V_1)}_{\omega\eta\eta'} &= \frac{8\sqrt{2}v}{\Lambda^4 F_0^2} (c^{(a)}_{us} + c^{(a)}_{ds}) \bar{g}^{(a)}_{V_1} \,, \\ g^{(V_1)}_{\phi\pi\eta} &= \frac{16v}{\sqrt{3}\Lambda^4 F_0^2} (c^{(a)}_{su} - c^{(a)}_{sd}) \, \bar{g}^{(a)}_{V_1} \,, & g^{(V_1)}_{\phi\eta\eta'} &= -\frac{16v}{\Lambda^4 F_0^2} (c^{(a)}_{su} + c^{(a)}_{sd}) \bar{g}^{(a)}_{V_1} \,. \end{aligned} \tag{2.31}$$

For the second operator in eq. (2.30) we observe that the resulting vector meson couplings $g^{(V_2)}_{vYX}$ equal the $g^{(V_1)}_{vYX}$ from eq. (2.31) if $c^{(a)}_{\psi\chi} \bar{g}^{(a)}_{V_2} = -c^{(a)}_{\chi\psi} \bar{g}^{(a)}_{V_1}$. The third operator in $\bar{X}^{(a)}_{\psi\chi}$ yields

$$\begin{aligned} g^{(V_3)}_{\rho\pi\eta} &= \frac{1}{\sqrt{3}} g^{(V_3)}_{\omega\eta\eta'} \,, & g^{(V_3)}_{\rho\eta\eta'} &= -\frac{4\sqrt{2}v}{3\Lambda^4 F_0^2} (c^{(a)}_{uu} - c^{(a)}_{dd}) \bar{g}^{(a)}_{V_3} \,, \\ g^{(V_3)}_{\omega\pi\eta} &= \frac{1}{\sqrt{3}} g^{(V_3)}_{\rho\eta\eta'} \,, & g^{(V_3)}_{\omega\eta\eta'} &= -\frac{4\sqrt{2}v}{3\Lambda^4 F_0^2} (c^{(a)}_{uu} + c^{(a)}_{dd}) \bar{g}^{(a)}_{V_3} \,, \\ g^{(V_3)}_{\phi\pi\eta} &= 0 \,, & g^{(V_3)}_{\phi\eta\eta'} &= \frac{16v}{3\Lambda^4 F_0^2} c^{(a)}_{ss} \bar{g}^{(a)}_{V_3} \,. \end{aligned} \tag{2.32}$$

Both eqs. (2.31) and (2.32) suggest that there is a correlation between $g_{\rho\pi\eta}$ and $g_{\omega\eta\eta'}$ as well as between $g_{\rho\pi\eta}$ and $g_{\omega\eta\eta'}$, but none of $g_{\phi\pi\eta}$ or $g_{\phi\eta\eta'}$ with the ρ couplings. However, this observation does not necessarily hold for higher orders in ToPeχPT or for operators derived from other LEFT sources. We continue with the couplings in eq. (2.32) as our central estimates and make use of the flavor relations implied therein.

Next, we consider the Lagrangian

$$\mathcal{L}_{v\gamma} = -\frac{e M_v^2}{g_{v\gamma}} A_\nu v^\nu \tag{2.33}$$

for the vector-meson conversion with known coupling constants $g_{v\gamma}$. As eq. (2.33) employs the photon field instead of the field strength tensor, it is not manifestly gauge invariant. In the end, this is a necessity to implement *strict* VMD for the isoscalar part of the form factor, avoiding an additional direct photon coupling. We can now evaluate the isoscalar

JHEP03(2024)059

contribution illustrated on the very right in figure 1, which, in agreement with eq. (2.4), gives rise to the matrix element

$$i\mathcal{M}^{(0)}_{XY} = e^2\,(P+p)_\mu\,F^{(0)}_{XY}(s)\,\bar{u}_r(p_{\ell^-})\gamma^\mu v_{r'}(p_{\ell^+})\,. \tag{2.34}$$

The corresponding isoscalar form factor, which is consistent with the high-energy behavior of the isovector part in eq. (2.27), finally reads

$$F^{(0)}_{XY}(s) \equiv \frac{\tilde{g}}{2g_{v\gamma}}\frac{M_v^2}{M_v^2 - s}\,, \tag{2.35}$$

where $\tilde{g}$ equals $g_{v\pi\eta}$ for $X = \eta$, $Y = \pi^0$ and $g_{v\eta\eta'}$ for $X = \eta'$, $Y = \eta$.

2.5 Discussion

With the results worked out in the previous sections we can evaluate the full contribution of the $X \to Y\gamma^*$ transition form factors by

$$F_{XY}(s) = F_1(s) + F_2(s) + F^{(1)}_{XY}(s) + F^{(0)}_{XY}(s)\,, \tag{2.36}$$

where each summand corresponds to one diagram in figure 1. Note that there is no way to distinguish between the four contributions in a sole measurement of the $X \to Y\ell^+\ell^-$ branching ratio.

Regarding F_1 and F_2, we observe that their NDA estimates in eqs. (2.14) and (2.18) yield roughly the same result, even without accounting for the uncertainty of NDA. Hence, there is no clear hierarchy between direct semi-leptonic contributions and C- and CP-violating photon–hadron couplings contributing to $X \to Y\ell^+\ell^-$. In future analyses, the sum $F_1 + F_2$ (which does not depend on s at leading order in ToPeχPT) may be replaced by a single constant parameter in a regression to hypothetical measurements of respective singly- or doubly-differential momentum distributions.

We remark in passing that *all* transition form factor contributions could be expected to undergo further hadronic corrections due to "initial-state interactions" of $\eta\pi$ and $\eta'\eta$ P-wave type, respectively. However, all corresponding phase shifts are expected to be tiny and the resulting effects to be hence utterly negligible: the $\eta\pi$ P-wave is strongly suppressed in the chiral expansion at low energies relative to $\eta\pi$ S-wave or $\pi\pi$ rescattering [70, 71], and resonances with quark-model-exotic quantum numbers $J^{PC} = 1^{-+}$ due to their C-odd nature will have a rather large mass [72]. We therefore do not consider any such corrections in this article.

Given the currently accessible experimental data and the missing information on the normalizations of F_1 and F_2, we henceforth focus on the contributions of $F^{(1)}_{XY}$ and $F^{(0)}_{XY}$. On the one hand, we are in a position to predict the latter with the input discussed in section 2.4. On the other hand, they provide new conceptual insights by directly relating ToPe forces in $X \to Y\pi^+\pi^-$ with $X \to Y\gamma^*$. Moreover, for simplicity we assume no significant cancellations among the individual contributions in eq. (2.36) throughout this manuscript. We leave the study of such a more complicated interplay between different mechanisms for future analyses, when more rigorous experimental bounds may be exploited for correlated constraints between them.

JHEP03(2024)059

3 Hadronic long-range effects: the isovector contribution

In this section we investigate the isovector contribution to the transition form factor $X \to Y\gamma^*$ based on the dispersive representations derived in section 2.4.1. Thus, we focus on C- and CP-odd contributions of the lowest-lying hadronic intermediate state, i.e., on the decay chain $X \to Y\pi^+\pi^- \to Y\gamma^*$.

3.1 The dispersive C- and CP-odd $X \to Y\pi^+\pi^-$ partial-wave amplitude

The formalism, results, and most of the notation are adopted from refs. [2, 3]. The latter uses a dispersive framework known as Khuri–Treiman equations [73] to access the three-body amplitude $X \to Y\pi^+\pi^-$ including its C- and CP-odd contributions. In this approach, a coupled set of integral equations is set up for the two-body scattering process and analytically continued to the physical realm of the three-body decay.

3.1.1 $\eta \to \pi^0\pi^+\pi^-$

The C- and CP-odd contributions to $\eta \to \pi^0\pi^+\pi^-$ read

$$\mathcal{M}^{\eta\pi}(s,t,u) = \mathcal{M}_0^{\eta\pi}(s,t,u) + \mathcal{M}_2^{\eta\pi}(s,t,u), \tag{3.1}$$

where the lower index denotes the *total* isospin of the three-body final state. Neglecting D- and higher partial waves, we can decompose these amplitudes in the sense of a reconstruction theorem [74–76] into single-variable functions $\mathcal{G}_{I_{\pi\pi}}(s)$, $\mathcal{H}_{I_{\pi\pi}}(s)$ with fixed *two-body* isospin $I_{\pi\pi}$ and relative angular momentum ℓ of the $\pi^+\pi^-$ state:

$$\begin{aligned}
\mathcal{M}_0^{\eta\pi}(s,t,u) &= (t-u)\mathcal{G}_1(s) + (u-s)\mathcal{G}_1(t) + (s-t)\mathcal{G}_1(u),\\
\mathcal{M}_2^{\eta\pi}(s,t,u) &= 2(u-t)\mathcal{H}_1(s) + (u-s)\mathcal{H}_1(t) + (s-t)\mathcal{H}_1(u) - \mathcal{H}_2(t) + \mathcal{H}_2(u).
\end{aligned} \tag{3.2}$$

Due to Bose symmetry the $I_{\pi\pi} = 1$ single-variable functions have $\ell = 1$ while the ones with $I_{\pi\pi} = 2$ have $\ell = 0$. Unitarity demands the single-variable functions to obey

$$\operatorname{disc}\mathcal{A}_{I_{\pi\pi}}(s) = 2i\,\sin\delta_{I_{\pi\pi}}(s)e^{-i\delta_{I_{\pi\pi}}(s)}\left(\mathcal{A}_{I_{\pi\pi}}(s) + \hat{\mathcal{A}}_{I_{\pi\pi}}(s)\right)\theta(s-4M_\pi^2), \tag{3.3}$$

with $\mathcal{A}_{I_{\pi\pi}} \in \{\mathcal{G}_{I_{\pi\pi}}, \mathcal{H}_{I_{\pi\pi}}\}$ and the $\pi\pi$ scattering phase shift $\delta_{I_{\pi\pi}}(s)$. The inhomogeneity $\hat{\mathcal{A}}_{I_{\pi\pi}}(s)$ contains left-hand-cut contributions induced by crossed-channel rescattering effects. In terms of the angular average

$$\langle z^n f\rangle := \frac{1}{2}\int_{-1}^{1}\mathrm{d}z\, z^n f\left(\tfrac{3r-s+z\kappa(s)}{2}\right), \tag{3.4}$$

with $3r \equiv s+t+u$, the $\hat{\mathcal{A}}_{I_{\pi\pi}}(s)$ explicitly read

$$\begin{aligned}
\hat{\mathcal{G}}_1(s) &= -\frac{3}{\kappa(s)}\left(3(s-r)\langle z\mathcal{G}_1\rangle + \kappa(s)\langle z^2\mathcal{G}_1\rangle\right),\\
\hat{\mathcal{H}}_1(s) &= \frac{3}{2\kappa(s)}\left(3(s-r)\langle z\mathcal{H}_1\rangle + \kappa(s)\langle z^2\mathcal{H}_1\rangle + 2\langle z\mathcal{H}_2\rangle\right),\\
\hat{\mathcal{H}}_2(s) &= \frac{1}{2}\left(9(s-r)\langle\mathcal{H}_1\rangle + 3\kappa(s)\langle z\mathcal{H}_1\rangle - 2\langle\mathcal{H}_2\rangle\right).
\end{aligned} \tag{3.5}$$

JHEP03(2024)059

For the $\mathcal{A}_{I_{\pi\pi}}(s)$ we employ dispersion relations with a minimal number of subtractions to ensure convergence. Assuming that in the limit of infinite s the phase shifts scale like $\delta_1(s) \to \pi$, $\delta_2(s) \to 0$ and the single-variable functions as $\mathcal{A}_1(s) = \mathcal{O}(s^{-1})$, $\mathcal{A}_2(s) = \mathcal{O}(s^0)$, we obtain

$$\begin{aligned}
\mathcal{G}_1(s) &= \Omega_1(s)\left(\varepsilon + \frac{s}{\pi}\int\limits_{4M_\pi^2}^{\infty}\frac{\mathrm{d}x}{x}\,\frac{\sin\delta_1(x)\hat{\mathcal{G}}_1(x)}{|\Omega_1(x)|\,(x-s)}\right),\\
\mathcal{H}_1(s) &= \Omega_1(s)\left(\vartheta + \frac{s}{\pi}\int\limits_{4M_\pi^2}^{\infty}\frac{\mathrm{d}x}{x}\,\frac{\sin\delta_1(x)\hat{\mathcal{H}}_1(x)}{|\Omega_1(x)|\,(x-s)}\right),\\
\mathcal{H}_2(s) &= \Omega_2(s)\frac{s}{\pi}\int\limits_{4M_\pi^2}^{\infty}\frac{\mathrm{d}x}{x}\,\frac{\sin\delta_2(x)\hat{\mathcal{H}}_2(x)}{|\Omega_2(x)|\,(x-s)}\,,
\end{aligned} \tag{3.6}$$

where here and in the following $M_\pi \equiv M_{\pi^\pm}$. The C-conserving SM amplitude for $\eta \to \pi^+\pi^-\pi^0$ is similarly described in terms of Khuri–Treiman amplitudes; these have been discussed extensively in the literature, see ref. [77] and references therein. The subtraction constants obtained by a fit to the Dalitz-plot distributions[6] of $X \to Y\pi^+\pi^-$ [79] yield [2, 3]

$$\varepsilon = i\,0.014(22)\,M_\pi^{-2}\,, \qquad \vartheta = i\,0.068(34)\times 10^{-3}\,M_\pi^{-2}\,. \tag{3.7}$$

These subtraction constants give rise to the real-valued isoscalar and isotensor couplings $g_0 = -2.8(4.5)\,\mathrm{GeV}^{-6}$ and $g_2 = -9.3(4.6)\cdot 10^{-3}\,\mathrm{GeV}^{-2}$ [2, 3], using

$$\varepsilon = -0.25i\,\mathrm{GeV}^4\,g_0\,, \qquad \vartheta = -0.38i\,g_2\,. \tag{3.8}$$

With the $\mathcal{A}_{I_{\pi\pi}}(s)$ defined above, the P-wave amplitude necessary to evaluate the $\eta \to \pi^0\gamma^*$ transition form factor is by definition, cf. eq. (2.25), given as

$$f_{\eta\pi}(s) = \mathcal{G}_1(s) + \hat{\mathcal{G}}_1(s) + \mathcal{H}_1(s) + \hat{\mathcal{H}}_1(s)\,, \tag{3.9}$$

whose dependence on $\mathcal{H}_2$ and $\hat{\mathcal{H}}_2$ is rather subtle and enters the definition of $\hat{\mathcal{H}}_1$ in eq. (3.5).

The transition form factor is fully determined by knowledge about the partial-wave amplitude $f_{XY}(s)$ and the pion vector form factor $F_\pi^V(s)$. These quantities are in turn fixed by the subtraction constants ε, ϑ, the S-wave $\pi\pi$ scattering phase shift δ_2 with isospin 2, and the P-wave $\pi\pi$ scattering phase shift δ_1 [80], respectively. The latter has to be used consistently in $f_{XY}(s)$ and $F_\pi^V(s)$, i.e., we use the same continuation to asymptotic s and omit the incorporation of inelasticities, which is beyond the scope of this work.

3.1.2 $\eta' \to \eta\pi^+\pi^-$

In the C-and CP-violating contribution to $\eta' \to \eta\pi^+\pi^-$ the three-body final state carries total three-body isospin 1. The respective amplitude can be decomposed as

$$\mathcal{M}^{\eta'\eta}(s,t,u) = (t-u)\mathcal{G}_{\pi\pi}(s) + \mathcal{G}_{\eta\pi}(t) - \mathcal{G}_{\eta\pi}(u); \tag{3.10}$$

[6]The latest BESIII data for $\eta \to \pi^+\pi^-\pi^0$ [78] is not included in refs. [2, 3] yet and has also not been added to our present analysis, as the statistical accuracy does not supersede that of ref. [79].

JHEP03(2024)059

see ref. [81] for the corresponding SM amplitude. The indices labeling the single-variable functions indicate which two particles contribute to the intermediate state of the scattering process. While the $\pi\pi$ intermediate state has the quantum numbers $I_{\pi\pi} = 1$, $\ell = 1$, $\eta\pi$ has $I_{\eta\pi} = 1$, $\ell = 0$. Both $\mathcal{G}_{\pi\pi}(s)$ and $\mathcal{G}_{\eta\pi}(s)$ fulfill the discontinuity equation as quoted in eq. (3.3). The inhomogeneities in this case are

$$\begin{aligned}\hat{\mathcal{G}}_{\pi\pi}(s) &= \frac{6}{\kappa_{\pi\pi}}\,\langle z_s \mathcal{G}_{\eta\pi}\rangle,\\ \hat{\mathcal{G}}_{\eta\pi}(t) &= -\langle \mathcal{G}_{\eta\pi}\rangle^{+} - \frac{3}{2}\left(r - t + \frac{\Delta}{3t}\right)\langle \mathcal{G}_{\pi\pi}\rangle^{-} + \frac{1}{2}\kappa_{\eta\pi}\langle z_t \mathcal{G}_{\pi\pi}\rangle^{-},\end{aligned} \tag{3.11}$$

where the cosine of the scattering angles in the s-channel is still given by the general expression eq. (2.26), $z_s \equiv z$, while the one in the t-channel reads

$$z_t = \frac{t\,(u-s) - \Delta}{t\,\kappa_{\eta\pi}(t)}\,, \qquad \text{with} \qquad \kappa_{\eta\pi}(t) = \frac{\lambda^{1/2}(t, M_{\eta'}^2, M_\pi^2)\,\lambda^{1/2}(t, M_\eta^2, M_\pi^2)}{t}\,. \tag{3.12}$$

In these equations we used the notation $\Delta \equiv (M_{\eta'}^2 - M_\pi^2)(M_\eta^2 - M_\pi^2)$. We additionally introduced two new types of angular averages, namely

$$\langle z^n f\rangle^{\pm} := \frac{1}{2}\int_{-1}^{1} \mathrm{d}z\, z^n f\Big(\tfrac{3r - t + z\kappa_{\eta\pi}(t) \pm \Delta/t}{2}\Big)\,. \tag{3.13}$$

Assuming the asymptotics $\delta_{\eta\pi}(t) \to \pi$ and $\mathcal{G}_{\pi\pi}(s) = \mathcal{O}(1/s)$, $\mathcal{G}_{\eta\pi}(t) = \mathcal{O}(t^0)$, the single-variable functions can be evaluated by

$$\begin{aligned}\mathcal{G}_{\pi\pi}(s) &= \Omega_{\pi\pi}(s)\left(\varrho + \frac{s}{\pi}\int_{s_{\text{th}}}^{\infty}\frac{\mathrm{d}x}{x}\frac{\sin\delta_{\pi\pi}(x)\hat{\mathcal{G}}_{\pi\pi}(x)}{|\Omega_{\pi\pi}(x)|\,(x-s)}\right),\\ \mathcal{G}_{\eta\pi}(t) &= \Omega_{\eta\pi}(t)\left(\zeta\, t + \frac{t^2}{\pi}\int_{t_{\text{th}}}^{\infty}\frac{\mathrm{d}x}{x^2}\frac{\sin\delta_{\eta\pi}(x)\hat{\mathcal{G}}_{\eta\pi}(x)}{|\Omega_{\eta\pi}(x)|\,(x-t)}\right).\end{aligned} \tag{3.14}$$

Here, the $\eta\pi$ S-wave phase shift from refs. [82, 83] has been employed. For the subtraction constants, the values

$$\varrho = -i\,0.04(12)\,M_\pi^{-2}\,, \qquad \zeta = i\,0.05(12)\,M_\pi^{-2}\,, \tag{3.15}$$

have been obtained by a regression to the Dalitz-plot distribution of $\eta' \to \eta\pi^+\pi^-$ [84]. In terms of the real-valued isovector coupling $g_1 = 0.7(1.0)\,\text{GeV}^{-2}$ and its leading correction $\delta g_1 = -5.5(7.3)\,\text{GeV}^{-2}$ [3], the subtraction constants read

$$\varrho = -3.5\cdot 10^{-3}\, i g_1\left(1 - 166.5\,\text{GeV}^2\,\delta g_1\right), \qquad \zeta = 0.76\, i g_1\left(1 - 0.65\,\text{GeV}^2\,\delta g_1\right). \tag{3.16}$$

Finally, the P-wave entering the $\eta' \to \eta\gamma^*$ transition form factor is given by

$$f_{\eta'\eta}(s) = \mathcal{G}_{\pi\pi}(s) + \hat{\mathcal{G}}_{\pi\pi}(s). \tag{3.17}$$

The dependence of $f_{\eta'\eta}$ on the S-wave amplitude $\mathcal{G}_{\eta\pi}$ is encoded in the angular averages in eq. (3.11).

JHEP03(2024)059

3.2 Computation of the isovector form factor $X \to Y\gamma^*$

When computing the transition form factors $F^{(1)}_{XY}$, it is advantageous to exploit the linearity of the three-body decay amplitudes $\mathcal{M}^{XY}$ in the subtraction constants. As mentioned in refs. [2, 3], the solutions of the Khuri–Treiman amplitudes can be represented by so-called basis solutions, which are independent of the subtraction constants and can be fixed once and for all before even carrying out a regression to data.

3.2.1 $\eta \to \pi^0\gamma^*$

The basis solutions for the P-wave amplitude $f_{\eta\pi}$ are defined by

$$f^{\varepsilon}_{\eta\pi}(s) \equiv \left[\mathcal{G}_1(s) + \hat{\mathcal{G}}_1(s)\right]\Big|_{\varepsilon=1}, \qquad f^{\vartheta}_{\eta\pi}(s) \equiv \left[\mathcal{H}_1(s) + \hat{\mathcal{H}}_1(s)\right]\Big|_{\vartheta=1}, \tag{3.18}$$

and illustrated in figure 4(top). The dimensionless $f^{\varepsilon}_{\eta\pi}$ corresponds to the isoscalar amplitude $\mathcal{M}^{\eta\pi}_0$, while $f^{\vartheta}_{\eta\pi}$ belongs to the isotensor one, i.e., to $\mathcal{M}^{\eta\pi}_2$. The partial waves have a singular character at pseudothreshold, i.e., the upper limit in s of the physical region in the $\eta \to \pi^0\pi^+\pi^-$ decay, which is contained in the inhomogeneities describing left-hand-cut contributions to the respective partial wave. Note that the form factor, after performing the dispersion integral over the discontinuity as in eq. (2.27), is perfectly regular at that point. Based on eq. (3.18), we can calculate the corresponding *basis form factors*

$$F^{\nu}_{\eta\pi}(s) = F^{(1)}_{\eta\pi}(s)|_{f_{\eta\pi}=f^{\nu}_{\eta\pi}}, \qquad \text{with} \qquad \nu \in \{\varepsilon, \vartheta\}, \tag{3.19}$$

which allow us to linearly decompose $F^{(1)}_{\eta\pi}$ according to

$$F^{(1)}_{\eta\pi}(s) = \varepsilon F^{\varepsilon}_{\eta\pi}(s) + \vartheta F^{\vartheta}_{\eta\pi}(s). \tag{3.20}$$

The $F^{\nu}_{\eta\pi}$ are pure predictions of our dispersive representation, independent of the subtraction constants. Our results for the basis solutions for the form factors are depicted in figure 4(bottom).

Let us have a look at the hierarchy of the two amplitudes contributing to $F^{(1)}_{\eta\pi}$. The plots in figure 4 show that the basis solutions for the isoscalar and isotensor contributions to the $\eta \to \pi^0\pi^+\pi^-$ P-wave amplitude are of the same order of magnitude, and so are, as a result, the corresponding basis form factors. But due to the vast difference in their normalizing subtraction constants, the term $\vartheta F^{\vartheta}_{\eta\pi}(s)$ is negligibly small in comparison to $\varepsilon F^{\varepsilon}_{\eta\pi}(s)$. The origin of this discrepancy is well understood [1–3]. The totally antisymmetric combination of P-wave single-variable functions in the isoscalar amplitude $\mathcal{M}^{\eta\pi}_0$, cf. eq. (3.2), leads to a strong kinematic suppression inside the Dalitz plot; for symmetry reasons alone, the amplitude is required to vanish along the three lines $s = t$, $t = u$, and $u = s$. As a result, the corresponding normalization ε is far less rigorously constrained from fits to experimental data [79] than the isotensor amplitude, which only vanishes for $t = u$. No such suppression occurs for the individual partial waves, or the transition form factors, be it in the ρ-resonance region or below, in the kinematic range relevant for the semi-leptonic decays studied here, where isoscalar and isotensor contributions show non-negligible, but moderate corrections to a ρ-dominance picture. We also remark that this subtle interplay demonstrates that the model-independent connection between Dalitz plots and transition form factors absolutely

JHEP03(2024)059

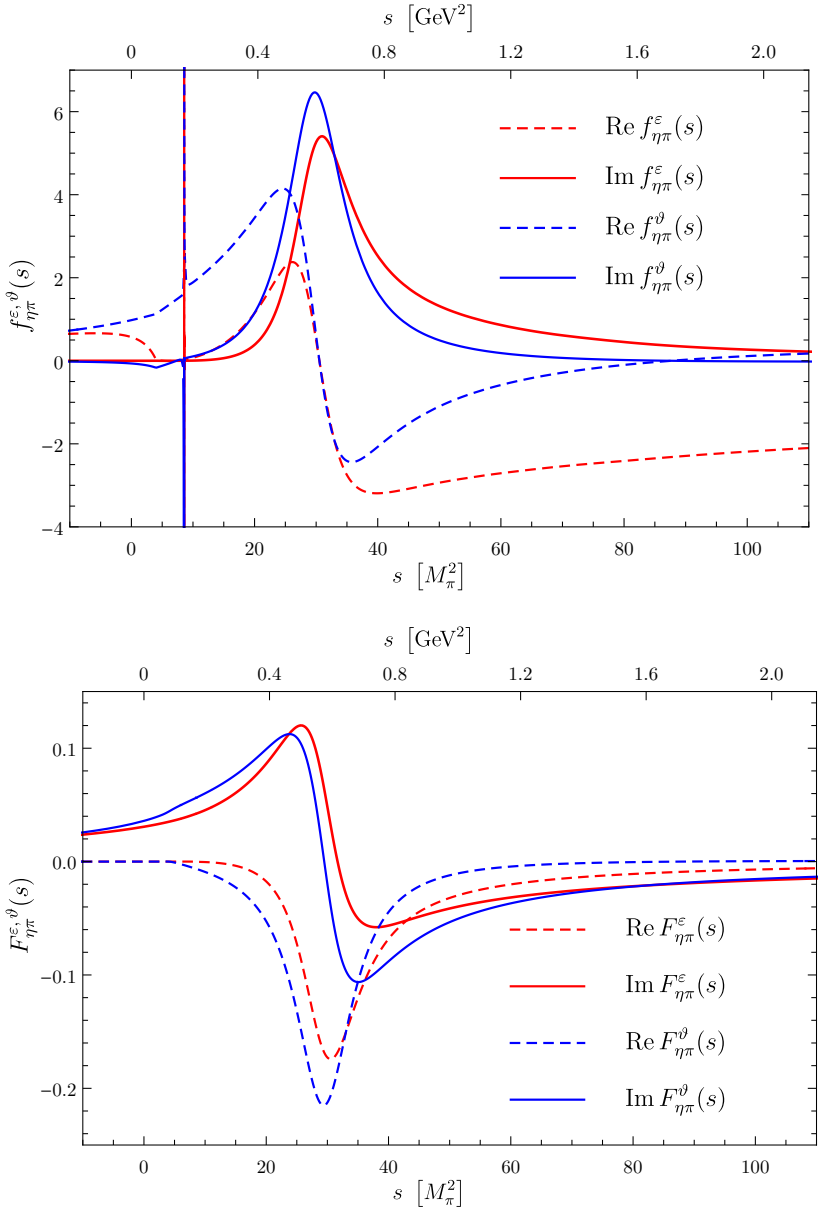

Figure 4. Basis solutions for the partial waves and form factors for the $\eta \to \pi^0$ transition. The partial-wave amplitudes $f^{\nu}_{\eta\pi}$ from eq. (3.18) are depicted in the upper panel; the singularity at the pseudothreshold $s = (M_\eta - M_{\pi^0})^2$ is clearly visible. These serve as an input to calculate the basis solutions of the transition form factors $F^{\nu}_{\eta\pi}(s)$ as defined in eq. (3.19) and shown in the lower panel.

requires the use of dispersion-theoretical methods—a low-energy effective theory such as chiral perturbation theory is insufficient for such extrapolations.

For the numerical evaluation of $F^{(1)}_{\eta\pi}$ we only consider the by far dominant source of error, i.e., the uncertainty of the subtraction constants entering the partial wave. As their errors are of the same order of magnitude as their corresponding central values, it is a good approximation to neglect all other sources of uncertainties, such as the variation of phase-shift input.

JHEP03(2024)059

3.2.2 $\eta' \to \eta\gamma^*$

We now turn the focus on the transition form factor $f_{\eta'\eta}$, whose basis solutions in terms of partial waves are defined as

$$f^{\varrho}_{\eta'\eta}(s) = \left[\mathcal{G}_{\pi\pi}(s) + \hat{\mathcal{G}}_{\pi\pi}(s)\right]\Big|_{\varrho=1,\,\zeta=0}\,, \qquad f^{\zeta}_{\eta'\eta}(s) = \left[\mathcal{G}_{\pi\pi}(s) + \hat{\mathcal{G}}_{\pi\pi}(s)\right]\Big|_{\varrho=0,\,\zeta=1}\,. \tag{3.21}$$

Using the $f^{\nu}_{\eta'\eta}$ we can define the basis from factors

$$F^{\nu}_{\eta'\eta}(s) = F^{(1)}_{\eta'\eta}(s)|_{f_{\eta'\eta}=f^{\nu}_{\eta'\eta}}\,, \quad \text{with} \quad \nu \in \{\varrho,\zeta\}\,, \tag{3.22}$$

and finally obtain the complete isovector form factor in explicit dependence on the subtraction constants by means of

$$F^{(1)}_{\eta'\eta}(s) = \varrho F^{\varrho}_{\eta'\eta}(s) + \zeta F^{\zeta}_{\eta'\eta}(s)\,. \tag{3.23}$$

The basis solutions for both partial waves and transition form factors are shown in figure 5.

3.3 Resonance couplings from analytic continuation

As both the partial waves $f_{XY}(s)$ and the resulting transition form factors $F^{(1)}_{XY}(s)$ have been constructed with the correct analytic properties, we can analytically continue them into the complex plane and onto the second Riemann sheet to extract resonance pole residues. The resonance in question is the $\rho(770)$; its residues can be interpreted as model-independent definitions of C-violating $\rho \to XY$ coupling constants. To this end, we recapitulate aspects of refs. [85, 86]. First, consider the discontinuity of the transition form factor in eq. (2.24) on the first Riemann sheet

$$F^{(1),\mathrm{I}}_{XY}(s+i\epsilon) - F^{(1),\mathrm{I}}_{XY}(s-i\epsilon) = \frac{i}{24\pi}\left(\sigma^{\pi}(s+i\epsilon)\right)^3 \left(F^{V,\mathrm{I}}_{\pi}(s+i\epsilon)\right)^* f^{\mathrm{I}}_{XY}(s+i\epsilon), \tag{3.24}$$

with

$$\sigma^{\pi}(s) \equiv \sqrt{\frac{4M_\pi^2}{s} - 1}\,, \qquad \sigma^{\pi}(s \pm i\epsilon) = \mp i\,\sigma_{\pi}(s)\,. \tag{3.25}$$

Using that the pion vector form factor fulfills Schwarz' reflection principle and demanding continuity of the scattering amplitudes when moving from one Riemann sheet to another, i.e.,

$$F^{(1),\mathrm{I}}_{XY}(s-i\epsilon) = F^{(1),\mathrm{II}}_{XY}(s+i\epsilon) \quad \text{and} \quad F^{V,\mathrm{I}}_{\pi}(s-i\epsilon) = F^{V,\mathrm{II}}_{\pi}(s+i\epsilon), \tag{3.26}$$

we obtain

$$F^{(1),\mathrm{II}}_{XY}(s+i\epsilon) = F^{(1),\mathrm{I}}_{XY}(s+i\epsilon) - \frac{i}{24\pi}\left(\sigma^{\pi}(s+i\epsilon)\right)^3 F^{V,\mathrm{II}}_{\pi}(s+i\epsilon)\, f^{\mathrm{I}}_{XY}(s+i\epsilon)\,. \tag{3.27}$$

Left- and right-hand side of eq. (3.27) depend on the same argument, such that, by analytic continuation, this relation can be applied in the whole complex plane. In particular, in the vicinity of the $\rho(770)$ pole, the transition form factors as well as the pion form factor on the second Riemann sheet behave as

$$F^{(1),\mathrm{II}}_{XY}(s)\,,\; F^{V,\mathrm{II}}_{\pi}(s) \propto \frac{1}{s_\rho - s}\,, \quad \text{with} \quad s_\rho = \left(M_\rho - i\frac{\Gamma_\rho}{2}\right)^2. \tag{3.28}$$

JHEP03(2024)059

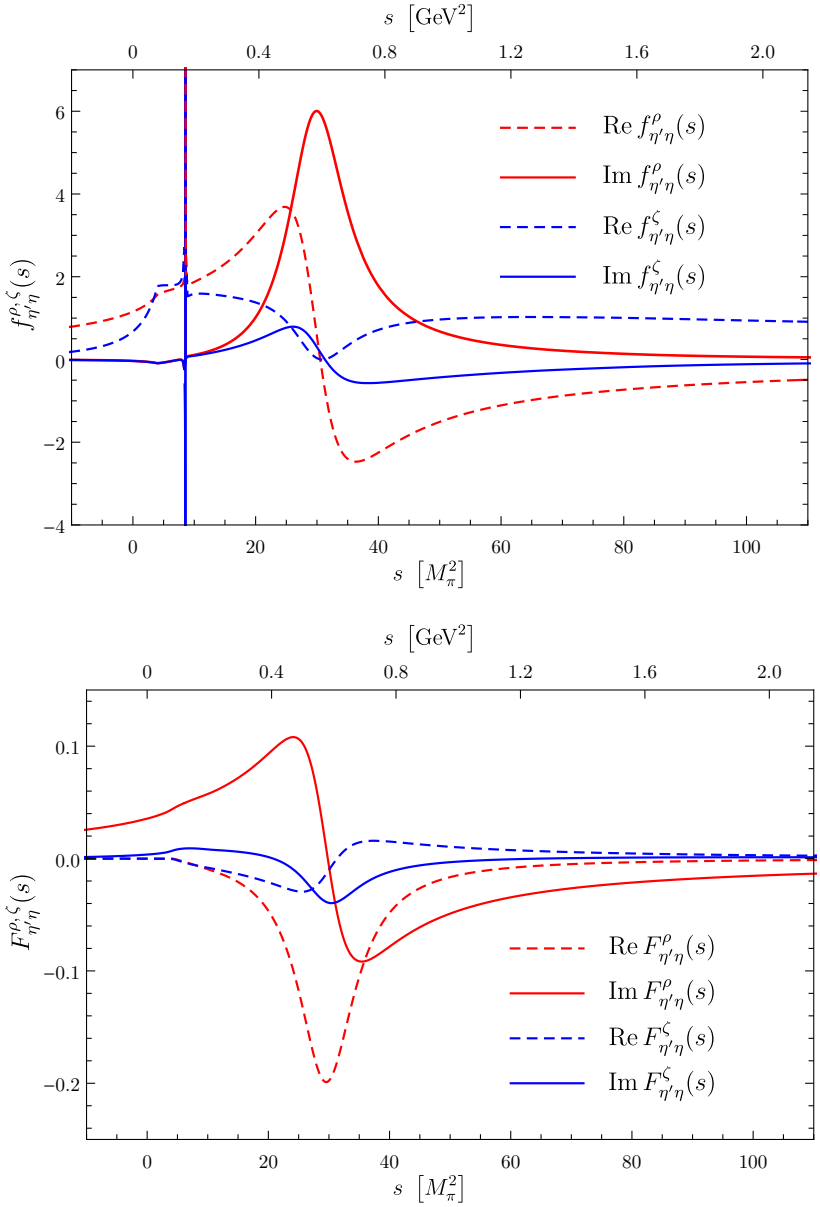

Figure 5. Basis solutions for the partial waves and form factors for the $\eta' \to \eta$ transition. The partial-wave amplitudes $f^{\nu}_{\eta'\eta}$ from refs. [2, 3] are depicted in the upper panel; again, the singularity at the pseudothreshold $s = (M_{\eta'} - M_\eta)^2$ can be seen. These serve as an input to calculate the basis solutions of the transition form factors $F^{\nu}_{\eta'\eta}(s)$ as defined in eq. (3.22) and shown in the lower panel.

The pole position s_ρ has been determined most accurately in ref. [43], using Roy-like equations for pion–pion scattering: $M_\rho = 763.7\,\text{MeV}$, $\Gamma_\rho = 146.4\,\text{MeV}$ (cf. also ref. [87]); for later use, we also quote the coupling constant to $\pi\pi$, $|g_{\rho\pi\pi}| = 6.01$, $\arg(g_{\rho\pi\pi}) = -5.3°$. We neglect the uncertainties in these parameters, as they are small compared to the ones fixing the partial waves f_{XY}. While $F_\pi^{V,\text{II}}$ is explicitly given in ref. [86], we can match $F_{XY}^{(1),\text{II}}$ to a VMD-type form factor similar to eq. (2.35), but with $g_{\rho YX}$, $g_{\rho\gamma}$, and M_ρ^2 instead of $\tilde{g}$, $g_{v\gamma}$, and M_v^2.

JHEP03(2024)059

Thus, in sufficient vicinity to the pole, we can write

$$F_\pi^{V,\mathrm{II}}(s) = \frac{g_{\rho\pi\pi}}{g_{\rho\gamma}} \frac{s_\rho}{s_\rho - s} \quad \text{and} \quad F_{XY}^{(1),\mathrm{II}}(s) = \frac{g_{\rho YX}}{2g_{\rho\gamma}} \frac{M_\rho^2}{s_\rho - s}. \tag{3.29}$$

If we evaluate eq. (3.27) near the pole s_ρ and insert eq. (3.29), we can compute the desired C-odd ρ-meson couplings by

$$g_{\rho YX} = \frac{g_{\rho\pi\pi}}{12\pi} \frac{s_\rho}{M_\rho^2} \sigma_\pi^3(s_\rho)\, f_{XY}^{\mathrm{I}}(s_\rho)\,. \tag{3.30}$$

The problem is therefore reduced to evaluating the partial wave f_{XY}^{I} on the first Riemann sheet at the pole position, a task for which the dispersive representations are perfectly suited. To clarify the dependence on subtractions or effective coupling constants and therefore separate the uncertainty in these from the precisely calculable dispersive aspects, we will once more make use of the decomposition in terms of basis functions.

We begin with the $\eta \to \pi^0$ transition form factor. The basis functions of the partial wave $f_{\eta\pi}$, evaluated at the ρ pole, result in

$$f_{\eta\pi}^{\varepsilon}(s_\rho) = -0.02 - 2.76i\,, \qquad f_{\eta\pi}^{\vartheta}(s_\rho) = 0.87 - 3.05i\,, \tag{3.31}$$

so that we obtain

$$f_{\eta\pi}(s_\rho) = \varepsilon f_{\eta\pi}^{\varepsilon}(s_\rho) + \vartheta f_{\eta\pi}^{\vartheta}(s_\rho) = \left[(-0.704 + i\,0.005)\,\mathrm{GeV}^4\, g_0 - (1.149 + i\,0.330) g_2\right], \tag{3.32}$$

where we made use of eq. (3.8). Employing of eq. (3.30) and finally inserting the values for the coupling constants g_0 and g_2 as extracted from the $\eta \to \pi^0\pi^+\pi^-$ Dalitz-plot asymmetry then yields

$$\begin{aligned} g_{\rho\pi\eta} &= \left[(-0.089 + i\,0.022)\,\mathrm{GeV}^4\, g_0 - (0.156 + i\,0.007)\, g_2\right] \\ &= \left[0.25(0.40) - i\,0.06(0.10)\right]\mathrm{GeV}^{-2}\,. \end{aligned} \tag{3.33}$$

Note that the isotensor contribution g_2 is negligible in the coupling $g_{\rho\pi\eta}$.

The analytic continuation of the basis partial wave for $f_{\eta'\eta}$ to the pole position of the ρ meson yields

$$f_{\eta'\eta}^{\varrho}(s_\rho) = 0.44 - 2.95i\,, \qquad f_{\eta'\eta}^{\zeta}(s_\rho) = -0.45 - 0.17i\,. \tag{3.34}$$

With eq. (3.16) we can hence express the analytically continued partial wave at the ρ pole by

$$f_{\eta'\eta}(s_\rho) = \varrho f_{\eta'\eta}^{\varrho}(s_\rho) + \zeta f_{\eta'\eta}^{\zeta}(s_\rho) = g_1 \left[(0.12 - i\,0.34) + (1.63 + i\,0.48)\,\mathrm{GeV}^2\,\delta g_1\right]. \tag{3.35}$$

In terms of this result, the ρ-meson coupling from eq. (3.30) results in

$$\begin{aligned} g_{\rho\eta\eta'} &= g_1 \left[(0.005 - i\,0.047) + (0.222 + i\,0.011)\,\mathrm{GeV}^2\,\delta g_1\right] \\ &= -\left[0.85(2.36) + i\,0.08(0.17)\right]\mathrm{GeV}^{-2}\,, \end{aligned} \tag{3.36}$$

where we considered correlated Gaussian errors for the couplings g_1 and δg_1.

JHEP03(2024)059

Note that the coupling constants in eq. (3.30) become inevitably complex-valued, thus spoiling the well-defined transformation under time reversal when compared to the tree-level coupling constants from ToPeχPT. This is neither surprising nor specific to the context of symmetry violation studied here: in the strong interactions, resonance couplings that are real in the narrow-width limit necessarily turn complex when defined model-independently via pole residues in the complex plane. However, this points towards the reason why these complex phases will be irrelevant when using symmetry arguments to estimate isoscalar contributions in the next section: for the narrow ω and ϕ resonances, they are negligible to far better accuracy; symmetry arguments within the vector-meson nonet are not applicable to their total widths. We will therefore simply omit the imaginary parts in the next section and relate the C-odd ω couplings required for the model of the isoscalar parts of the form factors to the real parts of the ρ coupling (of the same total isospin) only. Note furthermore that eqs. (3.33) and (3.36) still suggest the imaginary parts of $g_{\rho\pi\eta}$ and $g_{\rho\eta\eta'}$ to be rather small, such that the difference between real part and modulus, e.g., is negligible for our purposes.

4 Hadronic long-range effects: the isoscalar contribution

We now attempt to combine the findings of sections 2.4.2 and 3.3. We wish to access the couplings $\tilde{g}$, cf. eq. (2.35), by linking them to the $g_{\rho YX}$ discussed in the last section. In section 2.4.2 we found a ToPeχPT operator that, when considered separately, allows us — according to eq. (2.32) — to relate these couplings by $SU(3)$ symmetry. The vector-meson couplings with the same total isospin are found to be related by $g_{\omega\pi\eta} = 1/\sqrt{3}\, g_{\rho\eta\eta'}$ and $g_{\omega\eta\eta'} = \sqrt{3}\, g_{\rho\pi\eta}$, while $g_{\phi\pi\eta} = 0$ and $g_{\phi\eta\eta'}$ does *not* correlate with respective ρ couplings. However, the predictive power of flavor symmetry arguments does not hold in general for all operators. This leads to the shortcoming that we cannot fix the relative sign of the couplings, which becomes evident when comparing eqs. (2.31) and (2.32), and have to rely on NDA arguments to consider that there may be additional contributions to the couplings from linear combinations of Wilson coefficients, cf. eq. (2.31). An alternative approach would be to use NDA right away and drop the relative factors of $1/\sqrt{3}$ and $\sqrt{3}$, respectively, but this still leads to the same caveats.

4.1 $\eta \to \pi\ell^+\ell^-$

Possible contributions to the isoscalar form factor in $\eta \to \pi^0\ell^+\ell^-$ can originate from an ω or a ϕ intermediate state. In accordance with section 2.4.2, these enter the form factor in the linear combination

$$F_{\eta\pi}^{(0)}(s) \equiv \frac{g_{\omega\pi\eta}}{2g_{\omega\gamma}} \frac{M_\omega^2}{M_\omega^2 - s} + \frac{g_{\phi\pi\eta}}{2g_{\phi\gamma}} \frac{M_\phi^2}{M_\phi^2 - s}\,. \tag{4.1}$$

With our $SU(3)$ estimate $g_{\phi\pi\eta} = 0$ we can ignore the contribution of the ϕ. Dropping the latter is also justified from an NDA point of view: the difference of the two summands in eq. (4.1) is negligible compared to the uncertainty of NDA if $F_{\eta\pi}^{(0)}(s)$ is evaluated within the physical range. Therefore, we continue the estimation of the isoscalar contribution with the ω intermediate state only, for which we use $|g_{\omega\gamma}| = 16.7(2)$ [86].

JHEP03(2024)059

Relating $g_{\omega\pi\eta}$ to the ρ coupling of the same total isospin $I = 1$ and omitting the imaginary part for the reasons given above, we find

$$g_{\omega\pi\eta} \approx \frac{1}{\sqrt{3}} \mathrm{Re}\, g_{\rho\eta\eta'} = -0.49(1.36)\,\mathrm{GeV}^{-2} \quad \text{or} \quad |g_{\omega\pi\eta}| \lesssim 1.9\,\mathrm{GeV}^{-2}\,. \tag{4.2}$$

Throughout this manuscript we do not account for the numerically intangible uncertainties from our $SU(3)$ estimates or NDA. As neither of the latter fixes the sign of $|g_{\omega\pi\eta}|$, we have to content ourselves with its absolute value.

Note that retaining the imaginary part of $g_{\rho\eta\eta'}$ would have a negligible effect on the upper limit for $|g_{\omega\pi\eta}|$.

On the other hand, we can also place a bound on $|g_{\omega\pi\eta}|$ using the upper limit on the branching ratio of $\omega \to \eta\pi^0$ as determined by the Crystal Ball multiphoton spectrometer at the Mainz Microtron (MAMI) [88] and the Lagrangian in eq. (2.29). The partial decay width is found to be

$$\Gamma(\omega \to \eta\pi^0) = \frac{1}{192\pi M_\omega} |g_{\omega\pi\eta}|^2\, \lambda^{3/2}(M_\omega^2, M_\eta^2, M_{\pi^0}^2)\,. \tag{4.3}$$

With $\mathrm{BR}(\omega \to \eta\pi^0) < 2.3 \cdot 10^{-4}$ [88] and $\Gamma_\omega = 8.68$ MeV [42], we obtain the bound

$$|g_{\omega\pi\eta}| < 0.24\,\mathrm{GeV}^{-2}\,, \tag{4.4}$$

which is significantly more restrictive than the theoretical estimate for the bound on the coupling inferred from $g_{\rho\eta\eta'}$.

4.2 $\eta' \to \eta\ell^+\ell^-$

Similarly to the previous section, the isoscalar part of the form factor in $\eta' \to \eta\ell^+\ell^-$ can be written as

$$F^{(0)}_{\eta'\eta}(s) \equiv \frac{g_{\omega\eta\eta'}}{2g_{\omega\gamma}} \frac{M_\omega^2}{M_\omega^2 - s} + \frac{g_{\phi\eta\eta'}}{2g_{\phi\gamma}} \frac{M_\phi^2}{M_\phi^2 - s}\,. \tag{4.5}$$

With the same reasoning as above we henceforth drop the contribution of the ϕ and only take the ω into account. The numerical result for the corresponding vector meson coupling, which has total isospin $I = 0$, is

$$g_{\omega\eta\eta'} \approx \sqrt{3}\,\mathrm{Re}\, g_{\rho\pi\eta} = 0.43(0.69)\,\mathrm{GeV}^{-2} \quad \text{or} \quad |g_{\omega\eta\eta'}| \lesssim 1.1\,\mathrm{GeV}^{-2}\,. \tag{4.6}$$

Once more, the imaginary part of $g_{\rho\pi\eta}$ would yield just a minor contribution to the upper limit on $|g_{\omega\eta\eta'}|$ and can be neglected. We furthermore remark that the $\rho\pi\eta$ coupling also has an isotensor component, which, however, has a negligible effect, cf. eq. (3.33).

5 Results

With the theoretical apparatus at hand we are now able to predict upper limits on the decay widths

$$\Gamma(X \to Y\ell^+\ell^-) = \frac{\alpha^2}{8\pi M_X^3} \int_{4m_\ell^2}^{(M_X - M_Y)^2} \mathrm{d}s\, \lambda^{3/2}(s, M_X^2, M_Y^2)\, \sigma_\ell(s) \left(1 - \frac{\sigma_\ell^2(s)}{3}\right) |F_{XY}(s)|^2\,, \tag{5.1}$$

relying on the Dalitz-plot asymmetries in $X \to Y\pi^+\pi^-$ as the main input. As argued in section 2.5, we focus on the long-range contributions via hadronic intermediate states only, i.e., we set

$$F_{XY}(s) = F_{XY}^{(1)}(s) + F_{XY}^{(0)}(s)\,. \tag{5.2}$$

We disregard the contributions analyzed in sections 2.2 and 2.3 according to the discussion in section 2.5: these do not show interesting correlations with other ToPe processes, and absent significant cancellations, we can study the consequences of limit setting for the long-range hadronic effects alone. The corresponding transition form factors for the isovector and isoscalar contributions to $\eta \to \pi^0\gamma^*$ read

$$F_{\eta\pi}^{(1)}(s) = \varepsilon F_{\eta\pi}^{\varepsilon}(s) + \vartheta F_{\eta\pi}^{\vartheta}(s)\,, \qquad F_{\eta\pi}^{(0)}(s) = \frac{g_{\omega\pi\eta}}{2g_{\omega\gamma}}\frac{M_\omega^2}{M_\omega^2 - s}\,, \tag{5.3}$$

while the ones contributing to $\eta' \to \eta\gamma^*$ are

$$F_{\eta'\eta}^{(1)}(s) = \varrho F_{\eta'\eta}^{\varrho}(s) + \zeta F_{\eta'\eta}^{\zeta}(s)\,, \qquad F_{\eta'\eta}^{(0)}(s) = \frac{g_{\omega\eta\eta'}}{2g_{\omega\gamma}}\frac{M_\omega^2}{M_\omega^2 - s}\,. \tag{5.4}$$

The subtraction constants fixing the $F_{XY}^{(1)}$ are given in eqs. (3.7) and (3.15), the respective basis solutions F_{XY}^{ν} are depicted in figures 4 and 5, and the coupling constants $g_{\omega YX}$ entering the $F_{XY}^{(0)}$ are quoted in eqs. (4.4) and (4.6), respectively.

We have pointed out above that we have no means to assess the relative sign of the isoscalar contribution. To determine theoretical upper bounds, we investigate the parameter space spanned by the coupling constants and their uncertainties fixing

$$|F_{\eta\pi}|^2 = |F_{\eta\pi}^{(0)}|^2 + |F_{\eta\pi}^{(1)}|^2 + 2\,\mathrm{Re}\left(F_{\eta\pi}^{(0)}\,F_{\eta\pi}^{(1)*}\right) \tag{5.5}$$

and similarly for $F_{\eta'\eta}$.

5.1 $\eta \to \pi\ell^+\ell^-$

Based on the splitting of the absolute square of the transition form factor given in eq. (5.5), the branching ratios $\mathcal{B}_{\eta\to\pi^0 e^+e^-}$ and $\mathcal{B}_{\eta\to\pi^0\mu^+\mu^-}$ can be expressed in terms of the contributing BSM coupling constants g_0, g_2, and $g_{\omega\pi\eta}$ in the following way:

$$\begin{aligned}
\mathcal{B}_{\eta\to\pi^0 e^+e^-} &= 10^{-6}\Big(0.61\,\mathrm{GeV}^{12}\,g_0^2 + 2.20\,\mathrm{GeV}^{8}\,g_0\,g_2 + 1.99\,\mathrm{GeV}^{4}\,g_2^2 \\
&\qquad + 4.68\,\mathrm{GeV}^{8}\,g_0\,g_{\omega\pi\eta} + 8.44\,\mathrm{GeV}^{4}\,g_2\,g_{\omega\pi\eta} + 8.97\,\mathrm{GeV}^{4}\,g_{\omega\pi\eta}^2\Big)\,, \\
\mathcal{B}_{\eta\to\pi^0\mu^+\mu^-} &= 10^{-6}\Big(0.22\,\mathrm{GeV}^{12}\,g_0^2 + 0.81\,\mathrm{GeV}^{8}\,g_0\,g_2 + 0.76\,\mathrm{GeV}^{4}\,g_2^2 \\
&\qquad + 1.66\,\mathrm{GeV}^{8}\,g_0\,g_{\omega\pi\eta} + 3.10\,\mathrm{GeV}^{4}\,g_2\,g_{\omega\pi\eta} + 3.18\,\mathrm{GeV}^{4}\,g_{\omega\pi\eta}^2\Big)\,.
\end{aligned} \tag{5.6}$$

If we insert the maximum-range values $g_0 = (-2.8 - 4.5)\,\mathrm{GeV}^6$, $g_2 = (-9.3 - 4.6)\cdot 10^{-3}\,\mathrm{GeV}^{-2}$, and $|g_{\omega\pi\eta}| = 0.24\,\mathrm{GeV}^{-2}$, cf. section 3.1.1 and eq. (4.4), in eq. (5.6), we obtain the following conservative limits:

$$\begin{aligned}
&\mathcal{B}_{\eta\to\pi^0 e^+e^-}^{(1)} < 33\cdot 10^{-6}, \qquad \mathcal{B}_{\eta\to\pi^0 e^+e^-} < 41\cdot 10^{-6}, \qquad \mathcal{B}_{\eta\to\pi^0 e^+e^-}^{\mathrm{exp}} < 7.5\cdot 10^{-6}\,, \\
&\mathcal{B}_{\eta\to\pi^0\mu^+\mu^-}^{(1)} < 12\cdot 10^{-6}, \qquad \mathcal{B}_{\eta\to\pi^0\mu^+\mu^-} < 15\cdot 10^{-6}, \qquad \mathcal{B}_{\eta\to\pi^0\mu^+\mu^-}^{\mathrm{exp}} < 5\cdot 10^{-6}\,.
\end{aligned} \tag{5.7}$$

JHEP03(2024)059

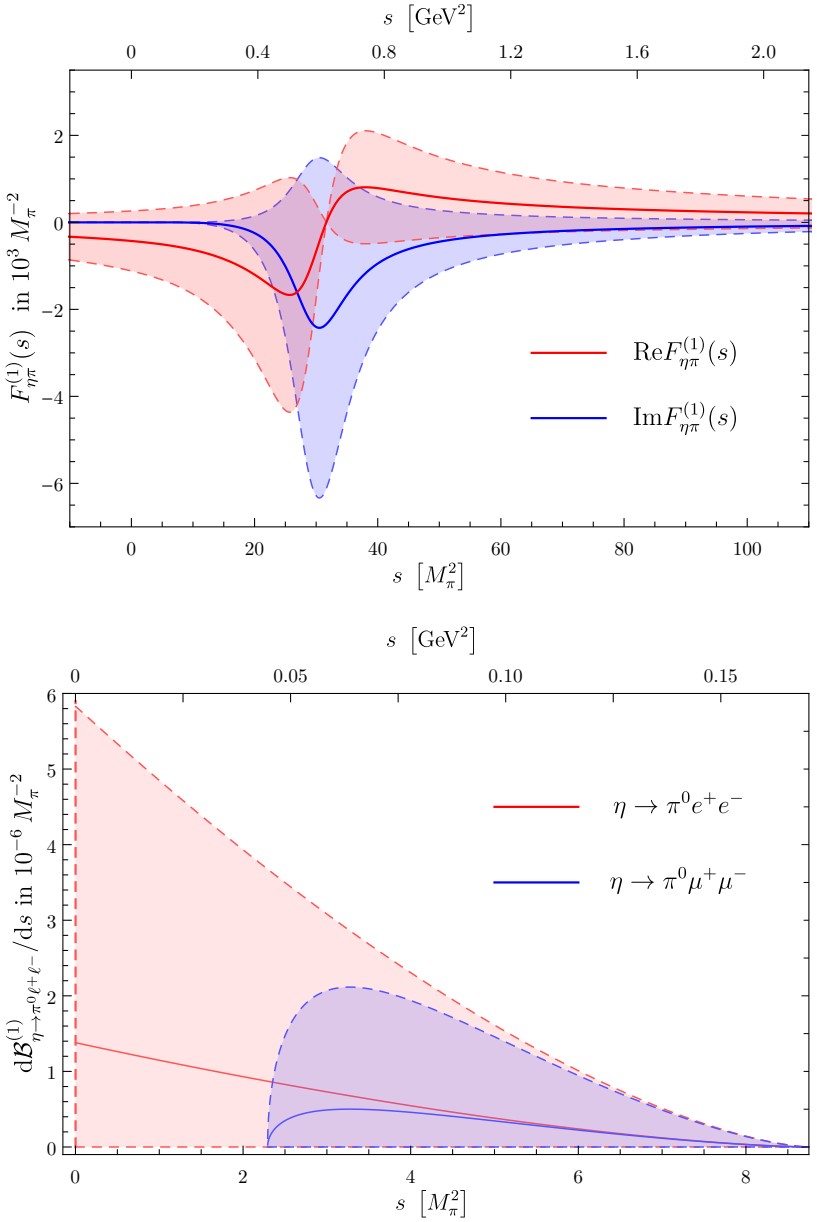

Figure 6. Spectrum of the isovector contribution to the form factor (top) and the corresponding differential decay distribution (bottom) for $\eta \to \pi^0 \ell^+ \ell^-$. The dashed lines mark the respective upper and lower limits stemming from the uncertainties of the subtraction constants in eq. (3.7). The physical ranges are in both cases restricted by $4m_\ell^2 \leq s \leq (M_\eta - M_\pi)^2$.

Here the first entry in each line corresponds to the isovector contribution and the second includes the isoscalar one in addition. Finally, the experimental results [19, 21], to be understood at 90% C.L., are quoted last (cf. table 1), which are smaller than our findings by a factor 5.5 and 3, respectively. The isovector contributions to the respective form factors and differential decay widths for the decay $\eta \to \pi\ell^+\ell^-$ are shown in figure 6. If the area enclosed by the error bands of the differential decay distribution is integrated, compatible but somewhat less conservative limit values result.

JHEP03(2024)059

BSM/hadronic coupl. constants		Empirical values via hadronic constraints	Limits derived in (5.6) from exp. bounds	Sensitivities in (5.6) from SM predictions
g_0	[GeV^{-6}]	$-2.8(4.5)$ [2]	(3.5 | 4.8)	$(5.0 \mid 5.8) \cdot 10^{-2}$
g_2	[GeV^{-2}]	$-9.3(4.6) \cdot 10^{-3}$ [2]	(1.9 | 2.6)	$(2.8 \mid 3.1) \cdot 10^{-2}$
$\lvert g_{\omega\pi\eta}\rvert$	[GeV^{-2}]	0.24 [88]	(0.9 | 1.3)	$(1.3 \mid 1.5) \cdot 10^{-2}$

Table 2. Empirical values, upper limits, and lower thresholds (sensitivities) of the BSM hadronic coupling constants g_0, g_2, and (the modulus of) $g_{\omega\pi\eta}$, derived (i) from the $\eta \to \pi^0\pi^+\pi^-$ Dalitz-plot asymmetries of ref. [2] and the empirical partial width of the decay $\omega \to \eta\pi^0$ [88], (ii) from the experimental upper bounds on the branching ratios $\mathcal{B}_{\eta\to\pi^0\ell^+\ell^-}$ given in table 1 for the dilepton pairs $(e^+e^- \mid \mu^+\mu^-)$, as calculated with aid of the relations (5.6) assuming that the other two coupling constants are vanishingly small, and (iii) as in (ii), but from the SM predictions listed in table 1.

Assuming that the other two coupling constants are negligible, the relations (5.6) can be used to derive upper bounds for, respectively, one of the three BSM coupling constants from the experimental limits of the branching ratios listed in table 1. In the same table, the Standard-Model predictions for the dilepton branching ratios based on the C-even two-photon mechanism [17] can be found. These can be used to calculate the lower threshold for the aforementioned coupling constants, at which the BSM scenario would no longer dominate the Standard-Model case. The upper bounds and the lower thresholds, which we refer to as sensitivities for the sake of simplicity, are listed in the third and fourth columns of table 2, respectively. The values to the left of the vertical bar refer to the case of e^+e^- dileptons, while the values to the right describe the results of the $\mu^+\mu^-$ case. In addition, we also list the empirical values of g_0 and g_2, derived via the $\eta \to \pi^0\pi^+\pi^-$ Dalitz-plot asymmetries in ref. [2], and the upper experimental bound (4.4) of $|g_{\omega\pi\eta}|$, derived from the partial decay width $\Gamma(\omega \to \eta\pi^0)$ [88], in the second column of table 2.

The empirical hadronic values of g_0 and $g_{\omega\pi\eta}$ are approximately of the same order of magnitude as the upper bounds calculated according to eq. (5.6). In contrast, the upper bound from eq. (5.6) is not competitive at all in the case of g_2, since it is more than two orders of magnitude larger than the (modulus of the) empirical value. Moreover, the latter is even smaller than the SM sensitivity for both decays $\eta \to \pi^0\ell^+\ell^-$, $\ell = e, \mu$. Therefore, these decays cannot be used to further constrain this parameter of C-odd, P-even η decays.

When making such comparisons, it must be kept in mind that the calculations of the upper bounds and lower threshold values are based on the strict assumption that the other two couplings are negligible. Should one of these three coupling constants be different from zero, it would be very unlikely that none of the other two should play any role.

In summary, the considered experiments for $\eta \to \pi^0\pi^+\pi^-$ and $\eta \to \pi^0\ell^+\ell^-$ have a quite similar sensitivity for ToPe forces of total isospin 0 as exemplified by the coupling g_0, despite the fact that asymmetries in the former are based on C-odd interferences and therefore scale *linearly* with a (small) BSM coupling [1, 4], while the latter is a rate that is suppressed to second order in a similar coupling. This is not so much due to a high sensitivity of the semi-leptonic decays, but rather to the strong suppression of g_0 in the $\eta \to \pi^0\pi^+\pi^-$ Dalitz

JHEP03(2024)059

plot. Comparing $\mathcal{B}^{(1)}_{\eta\to\pi^0\ell^+\ell^-}$ to $\mathcal{B}_{\eta\to\pi^0\ell^+\ell^-}$, our analysis suggests that the isoscalar form factor contributes roughly one quarter to the overall branching ratio. This reflects the more rigorous bound on the $\omega\to\eta\pi^0$ coupling, cf. eq. (4.4), compared to the limits inferred from the $\eta\to\pi^0\pi^+\pi^-$ Dalitz-plot asymmetries for the isovector part of the form factor.

As the experimental limits turn out to be more restrictive than our theoretical predictions for $\mathcal{B}^{(1)}_{\eta\to\pi^0\ell^+\ell^-}$, the empirical $\eta\to\pi^0\ell^+\ell^-$ decay widths [19, 21] can be used to refine the fit to the $\eta\to\pi^0\pi^+\pi^-$ Dalitz plot [79]. As long as the latter constrains the corresponding BSM couplings in a way that the form factor is dominated by the contribution of g_0, an improved regression to the full Dalitz plot is redundant. Instead we note that isoscalar (g_0) and isotensor (g_2) couplings in $\eta\to\pi^0\pi^+\pi^-$ are nearly uncorrelated [2] and turn the experimental limit for $\mathcal{B}^{(1)}_{\eta\to\pi^0e^+e^-}$ into the upper bound in table 2,

$$|g_0| < 3.5\,\text{GeV}^{-6}\,, \tag{5.8}$$

to be compared to the previous constraint $g_0 = -2.8(4.5)\,\text{GeV}^{-6}$ [2].

5.2 $\eta'\to\eta\ell^+\ell^-$

Proceeding in analogy to section 5.1, we obtain the following relations for the branching ratios in explicit dependence on the BSM couplings g_1, δg_1, and $g_{\omega\eta\eta'}$:

$$\begin{aligned}
\mathcal{B}_{\eta'\to\eta e^+e^-} &= 10^{-8}\Big(0.23\,\text{GeV}^4\,g_1^2 + 2.14\,\text{GeV}^6\,g_1^2\,\delta g_1 + 5.66\,\text{GeV}^8\,g_1^2\,\delta g_1^2 \\
&\qquad - 3.35\,\text{GeV}^4\,g_1\,g_{\omega\eta\eta'} - 17.76\,\text{GeV}^6\,g_1\delta g_1\,g_{\omega\eta\eta'} + 13.95\,\text{GeV}^4\,g^2_{\omega\eta\eta'}\Big)\,, \\
\mathcal{B}_{\eta'\to\eta\mu^+\mu^-} &= 10^{-8}\Big(0.13\,\text{GeV}^4\,g_1^2 + 1.05\,\text{GeV}^6\,g_1^2\,\delta g_1 + 2.25\,\text{GeV}^8\,g_1^2\,\delta g_1^2 \\
&\qquad - 1.62\,\text{GeV}^4\,g_1\,g_{\omega\eta\eta'} - 6.98\,\text{GeV}^6\,g_1\,\delta g_1\,g_{\omega\eta\eta'} + 5.43\,\text{GeV}^4\,g^2_{\omega\eta\eta'}\Big)\,.
\end{aligned} \tag{5.9}$$

If the maximum-range values $g_1 = (0.7{+}1.0)\,\text{GeV}^{-2}$, $g_1\delta g_1 = (-3.9{-}10.5)\,\text{GeV}^{-4}$ (interpreted as one effective coupling constant),[7] and $g_{\omega\eta\eta'} = (0.43 + 0.69)\,\text{GeV}^{-2}$, cf. section 3.1.2 and eq. (4.6), are inserted in eq. (5.9), the conservative estimates of the upper limits for the decays $\eta'\to\eta\ell^+\ell^-$ are[8]

$$\begin{aligned}
&\mathcal{B}^{(1)}_{\eta'\to\eta e^+e^-} < 11\cdot10^{-6}, \qquad \mathcal{B}_{\eta'\to\eta e^+e^-} < 14\cdot10^{-6}, \qquad \mathcal{B}^{\text{exp}}_{\eta'\to\eta e^+e^-} < 2.4\cdot10^{-3}\,, \\
&\mathcal{B}^{(1)}_{\eta'\to\eta\mu^+\mu^-} < 4.4\cdot10^{-6}, \qquad \mathcal{B}_{\eta'\to\eta\mu^+\mu^-} < 5.6\cdot10^{-6}, \qquad \mathcal{B}^{\text{exp}}_{\eta'\to\eta\mu^+\mu^-} < 15\cdot10^{-6}\,.
\end{aligned} \tag{5.10}$$

For these decays, our approximation for the isoscalar form factor loosens the limit on the isovector part by roughly a quarter. A depiction of the latter contribution to the form factor and differential decay width is given in figure 7. In contrast to the findings for $\mathcal{B}_{\eta\to\pi^0\ell^+\ell^-}$, our limits on $\mathcal{B}_{\eta'\to\eta\ell^+\ell^-}$ are more restrictive than the respective experimental ones.

Assuming that the other two coupling constants are negligible, the relations (5.9) can also be used to derive upper bounds for one of the three BSM coupling constants at a time,

[7] Note that the errors on g_1 and $g_1\delta g_1$ are almost perfectly anticorrelated [2, 3].

[8] For these branching ratios we use the total width $\Gamma_{\eta'} = 0.23\,\text{MeV}$ listed as *PDG average* in ref. [42]. Again the experimental branching ratios [19, 20] are to be understood at 90% C.L., cf. table 1, and the isovector part is designated with the upper index (1).

JHEP03(2024)059

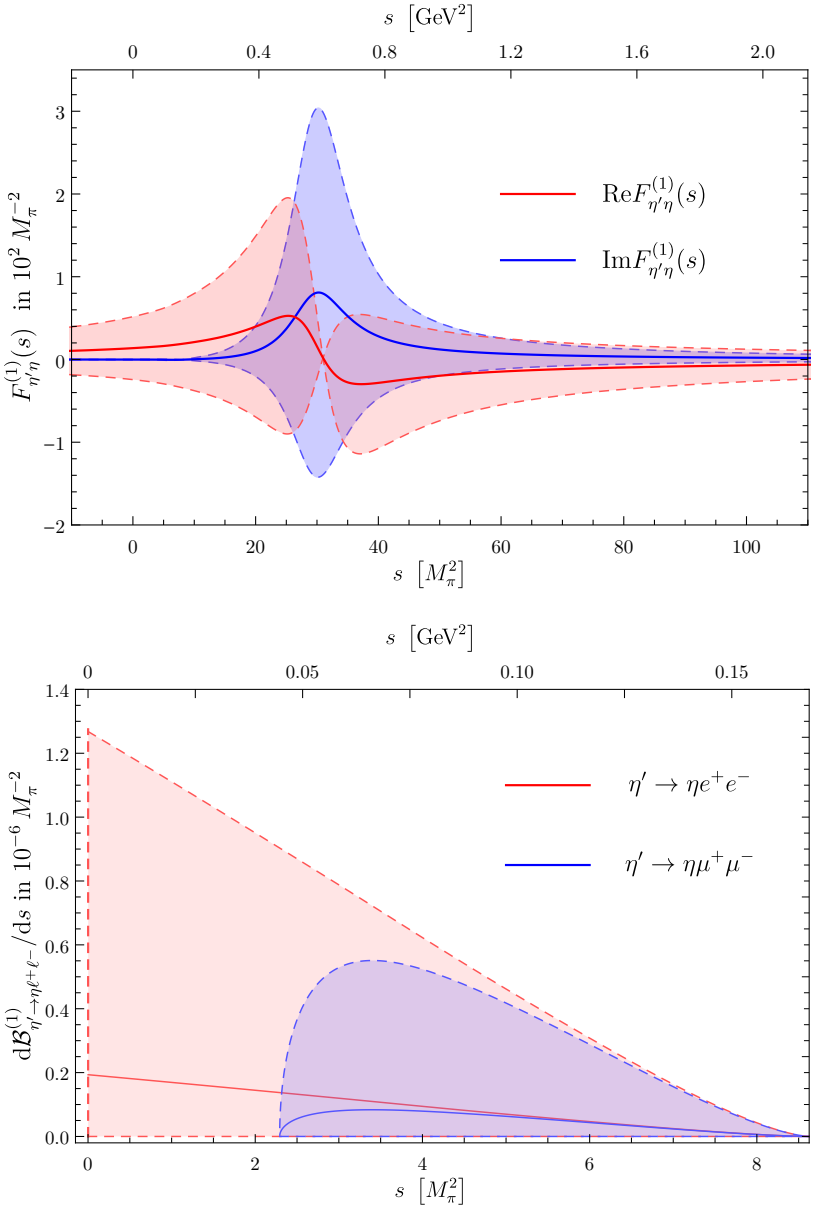

Figure 7. Spectrum of the isovector contribution to the form factor (top) and the corresponding differential decay distribution (bottom) for $\eta' \to \eta\ell^+\ell^-$. The dashed lines mark the respective upper and lower limits stemming from the uncertainties of the subtraction constants in eq. (3.15). The physical ranges are in both cases restricted by $4m_\ell^2 \leq s \leq (M_{\eta'} - M_\eta)^2$.

where the product $g_1\delta g_1$ can be non-zero even if g_1 itself is negligible. The experimental limits of the branching ratios and the Standard-Model predictions for the dilepton branching ratios based on the C-even two-photon mechanism [17] are taken from table 1. Again the latter are used to calculate the lower threshold for the above-mentioned coupling constants at which the BSM scenario would no longer dominate the Standard Model. The upper bounds and the lower thresholds (sensitivities) are listed in the third and fourth columns of the table 3, respectively. In the second column of table 3, we list the empirical values

JHEP03(2024)059

BSM/hadronic coupl. constants	Empirical values via hadronic constraints	Limits derived in (5.9) from exp. bounds	Sensitivities in (5.9) from SM predictions
g_1 [GeV^{-2}]	0.7(1.0) [3]	(1000| 110)	(0.49 | 0.45)
$g_1\delta g_1$ [GeV^{-4}]	−3.9(10.5) [3]	(210 | 26)	(0.10 | 0.11)
$g_{\omega\eta\eta'}$ [GeV^{-2}]	0.43(0.69) eq. (4.6)	(130 | 17)	(0.062 | 0.069)

Table 3. Empirical values, upper limits, and lower thresholds (sensitivities) of the BSM hadronic coupling constants g_1, $g_1\delta g_1$, and $g_{\omega\eta\eta'}$, derived (i) from the $\eta' \to \eta\pi^+\pi^-$ Dalitz-plot asymmetries of ref. [3] or computed from eq. (4.6), (ii) from the experimental upper bounds on the branching ratios $\mathcal{B}_{\eta'\to\eta\ell^+\ell^-}$ given in table 1 for the $(e^+e^- \mid \mu^+\mu^-)$ dilepton pairs, as calculated using the relations (5.9) assuming that the other two coupling constants are vanishingly small, and (iii) as in (ii), but from the SM predictions listed in table 1.

of g_1, of the product $g_1\delta g_1$, both derived via the $\eta' \to \eta\pi^+\pi^-$ Dalitz-plot asymmetries in ref. [3], and of $g_{\omega\eta\eta'}$, indirectly calculated via eq. (3.33) and eq. (4.6) from the corresponding $\eta \to \pi^0\pi^+\pi^-$ Dalitz-plot asymmetries [2, 3].

The empirical path via the $\eta' \to \eta\pi^+\pi^-$ Dalitz-plot asymmetries and eq. (4.6) to determine the BSM coupling constants is clearly preferable to the upper limit from the experimental bounds on the $\eta \to \pi^0\ell^+\ell^-$ decays, but still compatible with the lower thresholds from the C-even two-photon process of the Standard Model. However, the gaps between the empirical values and lower thresholds are smaller than in the η cases, especially for g_1.

6 Summary and outlook

In this work, we have studied the C- and CP-violating decays $\eta \to \pi^0\ell^+\ell^-$ and $\eta' \to \eta\ell^+\ell^-$, which can—from a phenomenological point of view—be driven by three different mechanisms. The first two of these are short-distance contributions induced by semi-leptonic four-point vertices and long-distance contributions caused by C- and CP-odd photon–hadron couplings. The only statements we can make about them is that they contribute as constants to respective transition form factors at leading order in ToPeχPT [4], that they cannot be distinguished by a sole measurement of the semi-leptonic decay widths, and that NDA estimates them to be of the same order of magnitude.

In contrast, the third mechanism, i.e., long-distance contributions induced by hadronic intermediate states, is conceptually more insightful. To access these contributions we have established dispersion relations for the isovector contribution to the transition form factors $\eta(\to \pi^0\pi^+\pi^-) \to \pi^0\gamma^*$ and $\eta'(\to \eta\pi^+\pi^-) \to \eta\gamma^*$. By construction, these form factors meet the fundamental requirements of analyticity and unitarity, solely relying on the dominant hadronic contribution of the P-waves in the C- and CP-odd $\eta \to \pi^0\pi^+\pi^-$ and $\eta' \to \eta\pi^+\pi^-$ amplitudes, which have been worked out in refs. [2, 3]. The non-perturbative predictions thereby obtained allow us to directly investigate the correlation between C-violating signals in different decays in a model-independent manner. By an analytic continuation of the C-odd $\eta \to \pi^0\pi^+\pi^-$ and $\eta' \to \eta\pi^+\pi^-$ P-wave amplitudes to the second Riemann sheet, we have extracted C-odd ρ-meson couplings to $\eta\pi^0$ and $\eta'\eta$. These two couplings can be related by

JHEP03(2024)059

total isospin and NDA to coupling constants entering the isoscalar contribution in a VMD model for $\eta' \to \eta\omega \to \eta\gamma^*$ and $\eta \to \pi^0\omega \to \pi^0\gamma^*$, respectively. However, the $\omega \to \eta\pi^0$ coupling could be bounded more precisely from the empirical limit on the corresponding partial width.

Accounting for these hadronic long-range effects only, we have predicted the corresponding upper limits on the semi-leptonic decay widths, relying on ToPe forces in the respective purely hadronic three-body decays as input. We observed that the currently most precise measurements of $\eta \to \pi^0\ell^+\ell^-$ have a similar sensitivity to isoscalar ToPe interactions as the measured Dalitz-plot asymmetries in $\eta \to \pi^0\pi^+\pi^-$, despite their different scaling with small BSM couplings. As we found the experimental limits for $\eta \to \pi^0\ell^+\ell^-$ to be more restrictive than our theoretically predicted ones, we were able to use the respective transition form factor as a constraint to sharpen the bounds on C violation in $\eta \to \pi^0\pi^+\pi^-$. On the other hand, both the isotensor coupling for C-odd η decays and the corresponding $\eta' \to \eta\ell^+\ell^-$ effects are more rigorously constrained indirectly from Dalitz-plot asymmetries. Finally, we have determined the best possible sensitivity to all C-odd hadronic couplings in semi-leptonic decays due to the Standard-Model background.

Given the relatively loose experimental bounds, we have largely eschewed concrete estimates of *theoretical* uncertainties in our limit setting. The dispersion relation used to connect hadronic and semi-leptonic decays are expected to work extremely well in the elastic approximation, with two-pion intermediate states only, for the relevant vector-isovector channel: comparable sum rules for SM processes typically work to better than 10% [37, 63]. This is the relevant accuracy for the relation between both types of C-odd effects. Neglected higher-order corrections in the chiral or large-N_c expansions, which may easily amount to 30% or so, only affect the interpretation of effective coupling constants on the mesonic level in terms of underlying LEFT or SMEFT operators [4].

Further perspectives on the decays $\eta \to \pi^0\ell^+\ell^-$ and $\eta' \to \eta\ell^+\ell^-$ could be opened by possible future measurements of the respective Dalitz-plot distributions. This would allow us to investigate actual C- and CP-odd observables, the Dalitz-plot asymmetries arising from the interference with the respective SM contributions. Such interference effects would, as the asymmetries in the hadronic η and η' decays, scale linearly with BSM couplings, however with likely less advantage in sensitivity due to the strongly suppressed SM amplitudes. Significant asymmetries can only be expected if, accidentally, C-even and -odd amplitudes happen to be of similar size. Still, due to synergy effects with other BSM searches in these decays, such as for weakly coupled light scalars [8], renewed experimental efforts are strongly encouraged.

Acknowledgments

We would like to thank Danny van Dyk for useful discussions. Financial support by the Avicenna-Studienwerk e.V. with funds from the BMBF, as well as by the DFG (CRC 110, "Symmetries and the Emergence of Structure in QCD"), is gratefully acknowledged.

JHEP03(2024)059

References

[1] S. Gardner and J. Shi, *Patterns of CP violation from mirror symmetry breaking in the $\eta \to \pi^+\pi^-\pi^0$ Dalitz plot*, *Phys. Rev. D* **101** (2020) 115038 [arXiv:1903.11617] [INSPIRE].

[2] H. Akdag, T. Isken and B. Kubis, *Patterns of C- and CP-violation in hadronic η and η' three-body decays*, *JHEP* **02** (2022) 137 [*Erratum ibid.* **12** (2022) 156] [arXiv:2111.02417] [INSPIRE].

[3] M.H. Akdag, *C and CP Violation in Light-Meson Decays*, Ph.D. thesis, University of Bonn, Bonn, Germany (2023) [DOI:10.48565/bonndoc-168].

[4] H. Akdag, B. Kubis and A. Wirzba, *C and CP violation in effective field theories*, *JHEP* **06** (2023) 154 [arXiv:2212.07794] [INSPIRE].

[5] J. Shi, *Theoretical Studies of C and CP Violation in $\eta \to \pi^+\pi^-\pi^0$ Decay*, Ph.D. thesis, Kentucky University, Lexington, U.S.A. (2017) [DOI:10.13023/etd.2020.388] [INSPIRE].

[6] S. Gardner and J. Shi, *Leading-dimension, effective operators with CP and C or P violation in Standard Model effective field theory*, to be published (2024).

[7] J.J. Sakurai, *Invariance Principles and Elementary Particles*, Princeton University Press (1964) [DOI:10.1515/9781400877874].

[8] L. Gan, B. Kubis, E. Passemar and S. Tulin, *Precision tests of fundamental physics with η and η' mesons*, *Phys. Rept.* **945** (2022) 1 [arXiv:2007.00664] [INSPIRE].

[9] J. Bernstein, G. Feinberg and T.D. Lee, *Possible C, T Noninvariance in the Electromagnetic Interaction*, *Phys. Rev.* **139** (1965) B1650 [INSPIRE].

[10] B. Barrett, M. Jacob, M. Nauenberg and T.N. Truong, *Consequences of C-Violating Interactions in η^0 and X^0 Decays*, *Phys. Rev.* **141** (1966) 1342 [INSPIRE].

[11] C.H. Llewellyn Smith, *The decay $\eta \to \pi^0 e^+ e^-$ with C conservation*, *Nuovo Cim. A* **48** (1967) 834 [*Erratum ibid.* **50** (1967) 374].

[12] T.P. Cheng, *C-Conserving Decay $\eta \to \pi^0 e^+ e^-$ in a Vector-Meson-Dominant Model*, *Phys. Rev.* **162** (1967) 1734 [INSPIRE].

[13] J. Smith, *C-Conserving Decay Modes $\eta \to \pi^0 e^+ e^-$ and $\eta \to \pi^0 \mu^+ \mu^-$*, *Phys. Rev.* **166** (1968) 1629.

[14] J.N. Ng and D.J. Peters, *The Decay of the η meson into $\pi\mu^+\mu^-$*, *Phys. Rev. D* **46** (1992) 5034 [INSPIRE].

[15] J.N. Ng and D.J. Peters, *A Study of $\eta \to \pi^0\gamma\gamma$ decay using the quark box diagram*, *Phys. Rev. D* **47** (1993) 4939 [INSPIRE].

[16] R. Escribano and E. Royo, *A theoretical analysis of the semileptonic decays $\eta^{(\prime)} \to \pi^0 l^+ l^-$ and $\eta' \to \eta l^+ l^-$*, *Eur. Phys. J. C* **80** (2020) 1190 [*Erratum ibid.* **81** (2021) 140] [*Erratum ibid.* **82** (2022) 743] [arXiv:2007.12467] [INSPIRE].

[17] H. Schäfer, M. Zanke, Y. Korte and B. Kubis, *The semileptonic decays $\eta^{(\prime)} \to \pi^0 \ell^+ \ell^-$ and $\eta' \to \eta \ell^+ \ell^-$ in the standard model*, *Phys. Rev. D* **108** (2023) 074025 [arXiv:2307.10357] [INSPIRE].

[18] R. Escribano, E. Royo and P. Sánchez-Puertas, *New-physics signatures via CP violation in $\eta^{(\prime)} \to \pi^0 \mu^+ \mu^-$ and $\eta' \to \eta \mu^+ \mu^-$ decays*, *JHEP* **05** (2022) 147 [arXiv:2202.04886] [INSPIRE].

[19] R.I. Dzhelyadin et al., *Search for Rare Decays of η and η' Mesons and for Light Higgs Particles*, *Phys. Lett. B* **105** (1981) 239 [INSPIRE].

JHEP03(2024)059

[20] CLEO collaboration, *Search for rare and forbidden η' decays*, *Phys. Rev. Lett.* **84** (2000) 26 [hep-ex/9907046] [INSPIRE].

[21] WASA-AT-COSY collaboration, *Search for C violation in the decay $\eta \to \pi^0 e^+ e^-$ with WASA-at-COSY*, *Phys. Lett. B* **784** (2018) 378 [arXiv:1802.08642] [INSPIRE].

[22] L. Gan and A. Gasparian, *Search of new physics via eta rare decays*, *PoS* **CD09** (2009) 048 [INSPIRE].

[23] GLUEX collaboration, *Eta Decays with Emphasis on Rare Neutral Modes: The JLab Eta Factory (JEF) Experiment*, https://www.jlab.org/exp_prog/proposals/14/PR12-14-004.pdf (2014).

[24] L. Gan, *Probes for Fundamental QCD Symmetries and a Dark Gauge Boson via Light Meson Decays*, *PoS* **CD15** (2015) 017 [INSPIRE].

[25] GLUEX collaboration, *Update to the JEF proposal (PR12-14-004)*, https://www.jlab.org/exp_prog/proposals/17/C12-14-004.pdf (2017).

[26] REDTOP collaboration, *The REDTOP project: Rare Eta Decays with a TPC for Optical Photons*, *PoS* **ICHEP2016** (2016) 812 [INSPIRE].

[27] REDTOP collaboration, *The REDTOP experiment*, arXiv:1910.08505 [INSPIRE].

[28] REDTOP collaboration, *The REDTOP experiment: Rare η/η' Decays To Probe New Physics*, arXiv:2203.07651 [INSPIRE].

[29] G. D'Ambrosio and G. Isidori, *CP violation in kaon decays*, *Int. J. Mod. Phys. A* **13** (1998) 1 [hep-ph/9611284] [INSPIRE].

[30] G. D'Ambrosio, G. Ecker, G. Isidori and J. Portoles, *The Decays $K \to \pi l^+ l^-$ beyond leading order in the chiral expansion*, *JHEP* **08** (1998) 004 [hep-ph/9808289] [INSPIRE].

[31] E.P. Shabalin, *Electric Dipole Moment of Quark in a Gauge Theory with Left-Handed Currents*, *Sov. J. Nucl. Phys.* **28** (1978) 75 [INSPIRE].

[32] I.B. Khriplovich, *Quark Electric Dipole Moment and Induced θ Term in the Kobayashi-Maskawa Model*, *Phys. Lett. B* **173** (1986) 193 [INSPIRE].

[33] A. Czarnecki and B. Krause, *Neutron electric dipole moment in the standard model: Valence quark contributions*, *Phys. Rev. Lett.* **78** (1997) 4339 [hep-ph/9704355] [INSPIRE].

[34] M. Pospelov and A. Ritz, *Electric dipole moments as probes of new physics*, *Annals Phys.* **318** (2005) 119 [hep-ph/0504231] [INSPIRE].

[35] BESIII collaboration, *Amplitude Analysis of the Decays $\eta' \to \pi^+\pi^-\pi^0$ and $\eta' \to \pi^0\pi^0\pi^0$*, *Phys. Rev. Lett.* **118** (2017) 012001 [arXiv:1606.03847] [INSPIRE].

[36] G. Köpp, *Dispersion calculation of the transition form-factor $f_{\pi\omega\gamma}(t)$ with cut contributions*, *Phys. Rev. D* **10** (1974) 932 [INSPIRE].

[37] S.P. Schneider, B. Kubis and F. Niecknig, *The $\omega \to \pi^0\gamma^*$ and $\phi \to \pi^0\gamma^*$ transition form factors in dispersion theory*, *Phys. Rev. D* **86** (2012) 054013 [arXiv:1206.3098] [INSPIRE].

[38] I.V. Danilkin et al., *Dispersive analysis of $\omega/\phi \to 3\pi, \pi\gamma^*$*, *Phys. Rev. D* **91** (2015) 094029 [arXiv:1409.7708] [INSPIRE].

[39] B. Kubis and F. Niecknig, *Analysis of the $J/\psi \to \pi^0\gamma^*$ transition form factor*, *Phys. Rev. D* **91** (2015) 036004 [arXiv:1412.5385] [INSPIRE].

[40] JPAC collaboration, *$\omega \to 3\pi$ and $\omega\pi^0$ transition form factor revisited*, *Eur. Phys. J. C* **80** (2020) 1107 [arXiv:2006.01058] [INSPIRE].

JHEP03(2024)059

[41] B. Kubis and R. Schmidt, *Radiative corrections in $K \to \pi\ell^+\ell^-$ decays*, *Eur. Phys. J. C* **70** (2010) 219 [arXiv:1007.1887] [INSPIRE].

[42] Particle Data Group collaboration, *Review of Particle Physics*, *PTEP* **2022** (2022) 083C01 [INSPIRE].

[43] R. García-Martín, R. Kamiński, J.R. Peláez and J. Ruiz de Elvira, *Precise determination of the f0(600) and f0(980) pole parameters from a dispersive data analysis*, *Phys. Rev. Lett.* **107** (2011) 072001 [arXiv:1107.1635] [INSPIRE].

[44] P. Sánchez-Puertas, *CP violation in η muonic decays*, *JHEP* **01** (2019) 031 [arXiv:1810.13228] [INSPIRE].

[45] T. Feldmann, *Quark structure of pseudoscalar mesons*, *Int. J. Mod. Phys. A* **15** (2000) 159 [hep-ph/9907491] [INSPIRE].

[46] R. Kaiser and H. Leutwyler, *Large N_c in chiral perturbation theory*, *Eur. Phys. J. C* **17** (2000) 623 [hep-ph/0007101] [INSPIRE].

[47] R. Escribano and J.-M. Frere, *Study of the η–η' system in the two mixing angle scheme*, *JHEP* **06** (2005) 029 [hep-ph/0501072] [INSPIRE].

[48] I.B. Khriplovich, *What do we know about T odd but P even interaction?*, *Nucl. Phys. B* **352** (1991) 385 [INSPIRE].

[49] R.S. Conti and I.B. Khriplovich, *New limits on T odd, P even interactions*, *Phys. Rev. Lett.* **68** (1992) 3262 [INSPIRE].

[50] J. Engel, P.H. Frampton and R.P. Springer, *Effective Lagrangians and parity conserving time reversal violation at low-energies*, *Phys. Rev. D* **53** (1996) 5112 [nucl-th/9505026] [INSPIRE].

[51] M.J. Ramsey-Musolf, *Electric dipole moments and the mass scale of new T violating, P conserving interactions*, *Phys. Rev. Lett.* **83** (1999) 3997 [*Erratum ibid.* **84** (2000) 5681] [hep-ph/9905429] [INSPIRE].

[52] A. Kurylov, G.C. McLaughlin and M.J. Ramsey-Musolf, *Constraints on T odd, P even interactions from electric dipole moments, revisited*, *Phys. Rev. D* **63** (2001) 076007 [hep-ph/0011185] [INSPIRE].

[53] R. Omnès, *On the Solution of certain singular integral equations of quantum field theory*, *Nuovo Cim.* **8** (1958) 316 [INSPIRE].

[54] V.L. Chernyak and A.R. Zhitnitsky, *Asymptotic Behavior of Hadron Form-Factors in Quark Model* (in Russian), *JETP Lett.* **25** (1977) 510 [INSPIRE].

[55] V.L. Chernyak and A.R. Zhitnitsky, *Asymptotics of Hadronic Form-Factors in the Quantum Chromodynamics* (in Russian), *Sov. J. Nucl. Phys.* **31** (1980) 544 [INSPIRE].

[56] A.V. Efremov and A.V. Radyushkin, *Asymptotical Behavior of Pion Electromagnetic Form-Factor in QCD*, *Theor. Math. Phys.* **42** (1980) 97 [INSPIRE].

[57] A.V. Efremov and A.V. Radyushkin, *Factorization and Asymptotical Behavior of Pion Form-Factor in QCD*, *Phys. Lett. B* **94** (1980) 245 [INSPIRE].

[58] G.R. Farrar and D.R. Jackson, *The Pion Form-Factor*, *Phys. Rev. Lett.* **43** (1979) 246 [INSPIRE].

[59] G.P. Lepage and S.J. Brodsky, *Exclusive Processes in Quantum Chromodynamics: Evolution Equations for Hadronic Wave Functions and the Form-Factors of Mesons*, *Phys. Lett. B* **87** (1979) 359 [INSPIRE].

JHEP03(2024)059

[60] G.P. Lepage and S.J. Brodsky, *Exclusive Processes in Perturbative Quantum Chromodynamics*, *Phys. Rev. D* **22** (1980) 2157 [INSPIRE].

[61] H. Leutwyler, *Electromagnetic form-factor of the pion*, in the proceedings of the *Continuous Advances in QCD 2002/ARKADYFEST*, Minneapolis, U.S.A. (2002) [DOI:10.1142/9789812776310_0002] [hep-ph/0212324] [INSPIRE].

[62] B. Ananthanarayan, I. Caprini and I.S. Imsong, *Implications of the recent high statistics determination of the pion electromagnetic form factor in the timelike region*, *Phys. Rev. D* **83** (2011) 096002 [arXiv:1102.3299] [INSPIRE].

[63] C. Hanhart et al., *The branching ratio $\omega \to \pi^+\pi^-$ revisited*, *Eur. Phys. J. C* **77** (2017) 98 [*Erratum ibid.* **78** (2018) 450] [arXiv:1611.09359] [INSPIRE].

[64] B. Lee, *Chiral dynamics*, *Cargese Lect. Phys.* **5** (1972) 119 [INSPIRE].

[65] O. Kaymakcalan and J. Schechter, *Chiral Lagrangian of Pseudoscalars and Vectors*, *Phys. Rev. D* **31** (1985) 1109 [INSPIRE].

[66] U.G. Meißner, *Low-Energy Hadron Physics from Effective Chiral Lagrangians with Vector Mesons*, *Phys. Rept.* **161** (1988) 213 [INSPIRE].

[67] P. Jain et al., *Realistic Pseudoscalar Vector Chiral Lagrangian and Its Soliton Excitations*, *Phys. Rev. D* **37** (1988) 3252 [INSPIRE].

[68] F. Klingl, N. Kaiser and W. Weise, *Effective Lagrangian approach to vector mesons, their structure and decays*, *Z. Phys. A* **356** (1996) 193 [hep-ph/9607431] [INSPIRE].

[69] M. Mai, U.-G. Meißner and C. Urbach, *Towards a theory of hadron resonances*, *Phys. Rept.* **1001** (2023) 1 [arXiv:2206.01477] [INSPIRE].

[70] V. Bernard, N. Kaiser and U.G. Meißner, *$\pi\eta$ scattering in QCD*, *Phys. Rev. D* **44** (1991) 3698 [INSPIRE].

[71] B. Kubis and S.P. Schneider, *The Cusp effect in $\eta' \to \eta\pi\pi$ decays*, *Eur. Phys. J. C* **62** (2009) 511 [arXiv:0904.1320] [INSPIRE].

[72] JPAC collaboration, *Determination of the pole position of the lightest hybrid meson candidate*, *Phys. Rev. Lett.* **122** (2019) 042002 [arXiv:1810.04171] [INSPIRE].

[73] N.N. Khuri and S.B. Treiman, *Pion-Pion Scattering and $K^\pm \to 3\pi$ Decay*, *Phys. Rev.* **119** (1960) 1115 [INSPIRE].

[74] J. Stern, H. Sazdjian and N.H. Fuchs, *What π-π scattering tells us about chiral perturbation theory*, *Phys. Rev. D* **47** (1993) 3814 [hep-ph/9301244] [INSPIRE].

[75] B. Ananthanarayan and P. Büttiker, *Comparison of πK scattering in* SU(3) *chiral perturbation theory and dispersion relations*, *Eur. Phys. J. C* **19** (2001) 517 [hep-ph/0012023] [INSPIRE].

[76] M. Zdráhal and J. Novotný, *Dispersive Approach to Chiral Perturbation Theory*, *Phys. Rev. D* **78** (2008) 116016 [arXiv:0806.4529] [INSPIRE].

[77] G. Colangelo, S. Lanz, H. Leutwyler and E. Passemar, *Dispersive analysis of $\eta \to 3\pi$*, *Eur. Phys. J. C* **78** (2018) 947 [arXiv:1807.11937] [INSPIRE].

[78] BESIII collaboration, *Precision measurement of the matrix elements for $\eta \to \pi^+\pi^-\pi^0$ and $\eta \to \pi^0\pi^0\pi^0$ decays*, *Phys. Rev. D* **107** (2023) 092007 [arXiv:2302.08282] [INSPIRE].

[79] KLOE-2 collaboration, *Precision measurement of the $\eta \to \pi^+\pi^-\pi^0$ Dalitz plot distribution with the KLOE detector*, *JHEP* **05** (2016) 019 [arXiv:1601.06985] [INSPIRE].

JHEP03(2024)059

[80] I. Caprini, G. Colangelo and H. Leutwyler, *Regge analysis of the $\pi\pi$ scattering amplitude*, *Eur. Phys. J. C* **72** (2012) 1860 [arXiv:1111.7160] [INSPIRE].

[81] T. Isken, B. Kubis, S.P. Schneider and P. Stoffer, *Dispersion relations for $\eta' \to \eta\pi\pi$*, *Eur. Phys. J. C* **77** (2017) 489 [arXiv:1705.04339] [INSPIRE].

[82] M. Albaladejo and B. Moussallam, *Form factors of the isovector scalar current and the $\eta\pi$ scattering phase shifts*, *Eur. Phys. J. C* **75** (2015) 488 [arXiv:1507.04526] [INSPIRE].

[83] J. Lu and B. Moussallam, *The $\pi\eta$ interaction and a_0 resonances in photon-photon scattering*, *Eur. Phys. J. C* **80** (2020) 436 [arXiv:2002.04441] [INSPIRE].

[84] BESIII collaboration, *Measurement of the matrix elements for the decays $\eta' \to \eta\pi^+\pi^-$ and $\eta' \to \eta\pi^0\pi^0$*, *Phys. Rev. D* **97** (2018) 012003 [arXiv:1709.04627] [INSPIRE].

[85] B. Moussallam, *Couplings of light $I = 0$ scalar mesons to simple operators in the complex plane*, *Eur. Phys. J. C* **71** (2011) 1814 [arXiv:1110.6074] [INSPIRE].

[86] M. Hoferichter, B. Kubis and M. Zanke, *Radiative resonance couplings in $\gamma\pi \to \pi\pi$*, *Phys. Rev. D* **96** (2017) 114016 [arXiv:1710.00824] [INSPIRE].

[87] G. Colangelo, J. Gasser and H. Leutwyler, *$\pi\pi$ scattering*, *Nucl. Phys. B* **603** (2001) 125 [hep-ph/0103088] [INSPIRE].

[88] A. Starostin et al., *Search for the charge-conjugation-forbidden decay $\omega \to \eta\pi^0$*, *Phys. Rev. C* **79** (2009) 065201 [INSPIRE].

JHEP03(2024)059